Evolution of the dynamics, area and ice production of the Amundsen Sea Polynya, Antarctica, 2016-2021

Grant J. Macdonald[1*], Stephen F. Ackley[1], Alberto M. Mestas-Nuñez[1] and Adrià Blanco-Cabanillas[2]

1) NASA Center for Advanced Measurements in Extreme Environments (CAMEE), University of Texas at San Antonio, San Antonio, TX 78249, USA
2) Department of Geography, University of Victoria, Victoria, BC V8W 2Y2, Canada
*Currently at (2)

Correspondence to: Grant J. Macdonald (*grantmacdonald@uvic.ca*)

Abstract. Polynyas are key sites of ice production during the winter and are important sites of biological activity and carbon sequestration during the summer. The Amundsen Sea Polynya (ASP) is the fourth largest Antarctic polynya, has recorded the highest primary productivity and lies in an embayment of key oceanographic significance. However, knowledge of its dynamics, and of sub-annual variations in its area and ice production, is limited. In this study we primarily utilize Sentinel-1 SAR imagery, sea ice concentration products and climate reanalysis data, along with bathymetric data, to analyze the ASP over the period November 2016 - March 2021. Specifically, we analyze (i) qualitative changes in the ASP's characteristics and dynamics, and quantitative changes in (ii) summer polynya area, (iii) winter polynya area and ice production. From our analysis of SAR imagery we find that ice produced by the ASP becomes stuck in the vicinity of the polynya and sometimes flows back into the polynya, contributing to its closure and limiting further ice production. The polynya forms westward off a persistent chain of grounded icebergs that are located at the site of a bathymetric high. Grounded icebergs also influence the outflow of ice and facilitate the formation of a 'secondary polynya' at times. Additionally, unlike some polynyas, ice produced by the polynya flows westward after formation, along the coast and into the neighboring sea sector. During the summer and early winter, broader regional sea ice conditions can play an important role in the polynya. The polynya opens in all summers, but record-low sea ice conditions in 2016/17 cause it to become part of the open ocean. During the winter, an average of 78% of ice production occurs in April-May and September-October, but large polynya events often associated with high, south-easterly or easterly winds can cause ice production throughout the winter. While passive microwave data or daily sea ice concentration products remain key for analyzing variations in polynya area and ice production, we find that the ability to directly observe and qualitatively analyze the polynya at a high temporal and spatial resolution with Sentinel-1 imagery provides important insights about the behavior of the polynya that are not possible with those datasets.

1. Introduction

Coastal polynyas, or 'latent heat polynyas' (and henceforth referred to simply as 'polynyas'), are sites of open water surrounded by sea ice and land, glacier ice or fast ice (Armstrong, 1972; Tamura et al., 2008; Park et al., 2018). These polynyas are distributed around the coast of Antarctica and are typically at fixed geographic locations each year. They develop because the ice that forms at these sites is regularly driven away by winds or ocean currents, creating an opening in the sea ice (Bromwich and Kurtz, 1984; Bromwich et al., 1993; 1998; Morales Maqueda et al. 2004; Sansiviero et al., 2017).

Between the Antarctic summer months of approximately November and March these open water sites tend to remain persistently ice-free. Among other factors, the combination of ice-free conditions, summer sunlight, and the availability of dissolved iron (e.g. Arrigo et al., 2008a; 2012; St-Laurent et al., 2017), enables large phytoplankton blooms to develop in polynyas during this summer period. These phytoplankton blooms fix carbon from dissolved carbon dioxide, some of which then sinks below the surface layer (Sweeney et al., 2003). As a result, the evolution of polynyas during the summer is considered a key factor in the primary productivity of the Southern Ocean, and consequently, also their role in the sequestration of carbon dioxide (the 'biological pump') (Arrigo et al., 2008b).

Between the Antarctic winter months of approximately April and October polynyas tend to be intermittently active and are smaller in area than in the summer. When a polynya does open during the winter, excess ocean heat is lost and new sea ice production takes place approximately immediately in the opened area. Winds (usually katabatic winds) or ocean currents later push the newly-produced sea ice away and open the polynya again, causing yet more ice to form. Repeated polynya 'events' produce new sea ice throughout the winter period and hence polynyas have been termed 'factories' of sea ice production (Kimura and Wakatsuchi, 2004; Assmann et al., 2005). Overall, polynyas are estimated to contribute around 10% of all Antarctic sea ice cover (Tamura et al., 2008; Nihashi and Oshima, 2015). Regionally, polynyas can play an even larger role in production. For example, the Ross Ice Shelf polynya is estimated to produce several cubic kilometers of ice annually, and along with the McMurdo Sound Polynya, may produce 20-50% of total sea ice in the region (Drucker et al., 2011). The polynya-produced ice then forms part of the pack ice, contributing to its characteristics and potentially further thickening due to deformation. For example, ice formed by the Terra Nova Bay polynya in the western Ross Sea had a mean thickness 3-4 times that of the central Ross Sea, with 80% of the ice contained in deformed ice and ridges (Rack et al., 2020). Consequently, understanding of polynya evolution through the winter is important for understanding ice production and sea ice characteristics in the Southern Ocean.

The Amundsen Sea Polynya (ASP), West Antarctica and the embayment in which it lies are of particular interest for several reasons. The polynya is situated in the embayment into which the Thwaites and Pine Island Glaciers terminate and undergo ocean-driven melting, making the oceanography of the embayment of special interest (IMBIE team, 2018; Rignot et al., 2019). The ASP is also known to be a key site of primary productivity in the summer, supporting rates of net primary production up to 2.5gC m^{-2} day^{-1}, the highest for any Antarctic polynya (Arrigo and Van Dijken, 2003; Arrigo et al., 2012), although the level of associated carbon sequestration is unclear (Lee et

al., 2017; St-Laurent et al., 2019). Additionally, the ASP has been highlighted as an important site for ice production. It has been identified as the fourth highest polynya in Antarctica in terms of area and ice production, only behind the Ross Ice Shelf, Cape Darnley, and Mertz polynyas (Tamura et al., 2008; 2016; Nihashi and Ohshima, 2015, Nihashi et al., 2017).

While there have been several recent studies of the ASP's evolution during the summer months (e.g. Arrigo et al., 2012; Stammerjohn et al., 2015, St-Laurent et al., 2019), knowledge of the ASP and its role in ice production during the winter is limited. Additionally, few studies during the summer have analyzed changes at the sub-monthly scale, and none have observed the polynya directly during cloudy conditions. Aside from one study that analyzed the ASP at the mean monthly scale (Tamura et al., 2016), studies that analyze ice production in the ASP during the winter have been limited to estimates of total annual ice production and mean annual area as part of broader-scale circum-Antarctic studies (Tamura et al., 2008; Nihashi and Ohshima, 2015; Nihashi et al., 2017). Other studies of the ASP during the winter have focused on other aspects of the polynya, such as iron and carbon fluxes (St-Laurent et al., 2019). There is a lack of studies of the polynya that characterize changes in the polynya's evolution and area through individual seasons. This is partly due to the difficulty of analyzing polynyas in detail during the polar night. However, the launch of the Sentinel-1 constellation of Synthetic Aperture Radar (SAR) - in full operation by May 2016 - enables us to directly observe the polynya during the polar night at a high spatial resolution. Additionally, during the summer light, SAR allows us to make observations regardless of cloud cover.

The overall goal of the work presented here is to improve knowledge of the behavior and evolution of the ASP, and thus to aid understanding of recent complex and poorly understood trends in Southern Ocean sea ice conditions. This in turn, will aid projections of future changes in Southern Ocean sea condition due to climate change, with important consequences for a range of processes such as Antarctic Ice Sheet stability (Banwell et al., 2017; Webber et al., 2017; Greene et al., 2018; Massom et al., 2018; Arthur et al., 2021) and ecosystem productivity (Grossman and Dieckmann, 1994; Ito et al., 2017). In particular we aim to provide the first qualitative description of the polynya's behavior based on direct observation. The three specific objectives of this paper are to, over the period November 2016 - March 2021, analyze seasonal and inter-annual (i) qualitative changes in the ASP's characteristics and dynamics, and quantitative changes in (ii) summer polynya area and (iii) winter polynya area and ice production. The main datasets used are Sentinel-1 SAR images, sea ice concentration products, and climate reanalysis data in the region of the ASP. Additionally, we analyze bathymetric data, and changes in the broader regional sea ice.

2. Study Site

The ASP is located at around ~72-73°S and 110-120°W in the Amundsen Sea embayment of the Southern Ocean in West Antarctica (Fig. 1). It is situated in a sector that exhibited an anomalous 40-year decreasing trend in sea ice extent until a 2007 minimum, since which there has been an increasing trend (Parkinson, 2019). The embayment also hosts an abundance of icebergs (Mazur et al., 2017; 2019; Bett et al., 2020). To the east, the polynya is bound by the Thwaites Iceberg Tongue (Iceberg B22A; Budge and Long, 2018) and a chain of icebergs grounded over Bear Ridge. To the south, when at its maximum extent, the polynya abuts the Dotson Ice Shelf and part of the

109 Getz Ice Shelf. Immediately east of the eastern boundary of the polynya is an area of ocean that is adjacent to

110 Thwaites Glacier and Pine Island Glacier. The neighboring 'Pine Island Polynya' forms along the coastal stretch

111 around this area and to the north. Westward coastal currents prevail in the area (Kim et al., 2016; St-Laurent et al.,

112 2019), that, along with easterly winds, carry icebergs (Koo et al., 2021) and sea ice into the adjacent sector or the

113 Amundsen Sea and eventually to the Ross Sea (Assmann et al., 2005).

114   The ASP opened every summer during the period 1979-2014 studied by Stammerjohn et al. (2015) and re-

115 tained some open polynya area through the winter period. Arrigo et al. (2012) found no significant secular trend in

116 mean summer open water area between 1997 and 2010, but Stammerjohn et al. (2015) did find the ASP's area in

117 December-February to increase overall over the period 1979-2014. They also noted that the site of the polynya

118 opening shifted to its current typical site adjacent to the Thwaites Glacier Tongue in 1993, having previously been

119 further to the west.

120   Synoptic-scale winds have been found to primarily determine the ASP's area and the timing of opening and

121 closure. Over the period 1997-2010, ASP area was greatest in the summers of 2002-03 and 2009-10, the years with

122 the largest monthly anomalies in easterly and southerly surface winds in the region, and smallest in 2003-04 when

123 there were anomalously high northerly and westerly winds (Arrigo et al., 2012). Polynya summer opening in No-

124 vember was associated with prevailing easterly or southeasterly winds, while closure in March was associated with

125 persistent southeasterly winds at a time when winds promote ice growth in open areas. The polynya was also found

126 to open for summer 16 $\pm$7 days earlier at the end of the period 1979/80-2013/14 than the beginning (Stammerjohn

127 et al., 2015).

128   During the winter, the ASP active area was estimated to have a daily mean of 7700 ± 3600 km^2 for the pe-

129 riod March-October, 2003-11, as estimated by mapping thin-ice thickness from Advanced Microwave Scanning Ra-

130 diometer for EOS [Earth Observing System] (AMSR-E) data (Nihashi and Ohshima, 2015). Annual ice production

131 volume has been estimated as 92 ± 16 km^3 for the period 1992-2001 (Tamura et al., 2008) and 123 ± 24 km^3 for the

132 period 1992-2013 (Tamura et al., 2016) by mapping thin-ice thickness using Special Sensor Microwave/Imager

133 (SSM/I) data and calculating heat flux using SSM/I and surface atmospheric data. Nihashi et al., 2017 estimated an-

134 nual volume of ice production, as 90 ± 13 km^3 for the period 2003-10, and 90 ± 17 km^3 for the period 2013-15 , by

135 mapping thin-ice thickness and estimating heat fluxes using AMRS-E and AMSR2 data, respectively.

136
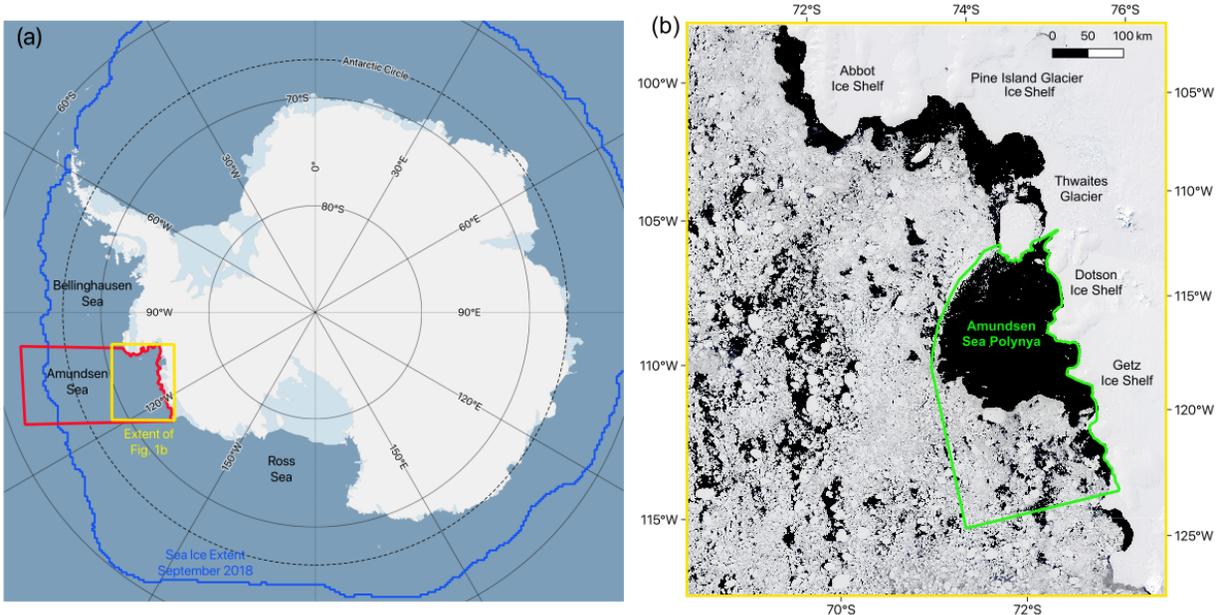
Fig. 1. (a) The location of the Amundsen Sea and our study sites within the context of Antarctica and the Southern Ocean. The background image is from Quantarctica (Matsuoka et al., 2021); (b) The location of the ASP within the Amundsen Sea embayment. The green boundary indicates the area defined as the 'ASP study area' for the purpose of calculating winter polynya area and ice production. The background image is a true-color MODIS image from 12 December 2020.

3. Data & Methods

3.1 Qualitative analysis of the ASP's evolution

In order to qualitatively characterize the seasonal and interannual evolution of the ASP we use Sentinel-1 SAR imagery. Qualitative visual analysis allows us to identify dynamics that are not easy or possible to identify and/or describe with quantitative data. Sentinel-1 is a constellation of two satellites, A and B, that were launched by the European Space Agency (ESA) in 2014 and 2016, respectively. The satellite collects radar backscatter imagery in the C-band which allows observations of sea ice and the ocean during cloudy conditions and the polar night.

For our analysis we produced a time-lapse animation in Google Earth Engine using all Sentinel-1 extra-wide swath (EW) mode, Ground Range Detected (GRD) images over the study site described in section 2 and its surroundings for the period November 2016 to March 2021. This period was chosen because it includes all the complete summer (November-March) and winter (April-October) periods during which both satellites A and B of the Sentinel-1 SAR constellation have been active. The EW mode was primarily designed for sea ice and polar zones and collects images over a wider area than other modes. EW images are available in 20m x 40m spatial resolution and all images were resampled to 40 m grid spacing. Of four available band combinations (VV, HH, VV+VH, and HH+HV), we use the HH band because most of the images contain this band. Google Earth Engine applies a series of pre-processing steps to Sentinel-1 images (https://developers.google.com/earth-engine/guides/sentinel1): 1) application of orbit file, 2) GRD border noise removal, 3) thermal noise removal, 4) radiometric calibration and 5) orthorectification. Images are also converted to decibels (dB). Using these images, we created a time-lapse animation using Google Earth Engine. This time-lapse included at least partial coverage of the study area for 56 days in 2016,

163   359 days in 2017, 341 days in 2018, 317 days in 2019, 329 days in 2020 and 85 days in 2021. In order to analyze

164   particular images in detail, the images were also downloaded from the Alaska Satellite Facility (asf.alaska.edu) and

165   processed in ESA's 'SNAP' toolbox. SNAP was used to crop the images, apply radiometric correction (gamma-

166   nought), apply a Lee (7 x7) speckle filter and perform ellipsoid correction and map projection, projecting to an Ant-

167   arctic polar stereographic projection. Images were also converted to decibels. The images were then loaded into

168   QGIS (QGIS.org, 2021) for analysis.

169   Qualitative analysis was carried out by visually analyzing the time-lapse videos and images of interest, not-

170   ing changes in the state of the polynya and ice in the region. Visual analysis is possible by analyzing changes in the

171   backscatter signal's texture, pattern and tone and because of the distinct backscatter characteristics of open water,

172   older icepack and different types of thin sea ice. The motion of the ice between images also helped in the identifica-

173   tion of polynya events. Numerous previous studies have noted the ability to observe polynya activity and visually

174   identify polynya opening and the drift of ice with SAR imagery and Sentinel-1 in particular (e.g. Hollands and

175   Dierking, 2016; Dai et al., 2020; Moore et al., 2021). Visual qualitative analysis of SAR imagery also forms an im-

176   portant part of, for example, the Environment Canada's production of sea ice charts (Environment Canada, 2005).

177   Typically, open ocean water has a low backscatter and appears dark, while thicker, older icepack has a relatively

178   high backscatter and appears bright and more granular (we refer to all ice not produced by the ASP as 'pack ice')

179   (Fig. 2a-b). Recently-formed polynya-produced ice has an intermediate backscatter (Fig. 2a). Frazil ice, that may

180   form when a polynya opens up and the open ocean begins to freeze, typically forms in distinct bands of varying

181   brightness (Fig. 2c-d) although it may also form in a 'swirl' or other forms. Open ocean may also appear bright dur-

182   ing high winds, but it is typically clear from the pattern, tone and texture, and the context of the image whether it is

183   an area of ice-free open ocean, or an area of pack ice or active polynya. Incidence angle also influences backscatter

184   and should be considered in a quantitative study of backscatter but it is not generally considered a significant imped-

185   iment in the ability to qualitatively analyses images for this study's purpose, with visual analysis dependent on a

186   number of factors. Note that what we refer to as 'active' polynya area during the winter will typically be filled with

187   thin, newly-forming frazil ice.

188   Given the role grounded icebergs play in bounding the ASP, we also downloaded the 'BedMachine Antarc-

189   tica V2' sea floor topography dataset for our study area to examine alongside our qualitative analysis. This dataset

190   was downloaded from the NSIDC (https://nsidc.org/data/nsidc-0756) and has a grid spacing of 500 x 500 m

191   (Morlighem et al., 2020).

192   We also use our analysis of the imagery to assess the approximate day of summer polynya 'opening' and

193   'closing'. We deem the polynya to be open for the summer when the open polynya area is primarily free of active

194   ice production, and the day of summer closing to be when the whole open polynya is subject to ice production.

195

196   **3.2 Daily polynya area**

197   In order to analyze seasonal and interannual changes in polynya area in summer and winter, daily sea ice

198   concentration (SIC) for the study region was downloaded from the University of Bremen's sea ice data center

199   (seaice.uni-bremen.de). The data was separated into five summer periods from November to March (2016/17,

200 2017/18, 2018/19, 2019/20 2020/21) and four winter periods from April to October (2017, 2018, 2019, 2020). This

201 time period was focused on because it coincides with the period for which there is Sentinel-1 A and B data. During

202 the winter we use the term 'active polynya' for areas that we include in the polynya, where an opening has been cre-

203 ated and new ice production is taking place. During the winter we expect thin, frazil ice to immediately begin form-

204 ing when an opening is created (e.g. Nakata et al., 2019; 2021), and thus we prefer the term 'active' to 'open' ocean.

205 We begin our winter period in April rather than March because analysis of the Sentinel-1 imagery suggests ice pro-

206 duction is not active across the open polynya at the beginning of March. The sea ice concentration product was pro-

207 cessed by the University of Bremen using the ARTIST Sea Ice (ASIC) algorithm (Spreen et al, 2008) applied to

208 AMSR-2 data. AMSR-2 was launched onboard the Japan Aerospace Exploration Agency's (JAXA) Global Change

209 Observation Mission – Water (GCOM-W) satellite in July 2012.

210   We used version 5.4 of the Antarctic-wide, daily sea ice concentration product with no land mask, pro-

211 cessed to 3.125 km grid spacing. This is of a higher-resolution than data previously used to analyze polynya area in

212 the region. For example, Arrigo et al., (2012) used SSM/I data with 6.25 km grid spacing for their study of summer

213 polynya area. Nihashi et al. (2017) used AMSR-E data with 6.25 km grid spacing for their estimates of ice produc-

214 tion. Tamura et al. (2008; 2016) also used SSM/I data, with 12.5 km grid spacing, for estimates of ice production.

215 Stammerjohn et al. (2015) used Bootstrap SIC data with 25 km grid spacing for their analysis of summer polynya

216 area. However, with our higher-resolution data (3.125 km) there remain limitations in using data with such a scale to

217 measure something that can vary on a meterscale. It has been estimated that the ice concentration error in our

218 AMSR-2 dataset is 25% at 0% SIC, decreasing to <10% error for SIC over 65% and 5.7% error at 100% SIC

219 (Spreen et al., 2008). It is also noted that the SIC data is known to underestimate SIC where there is thin ice, but as

220 we define an active polynya as including thin ice, this is not likely to lead to substantial misclassification of active

221 polynya areas. Data was available for all days in our study period apart from one day in 2019 (1 September).

222   After each day's data was downloaded as a geotiff, it was cropped to the 70 660 km^2 ASP study area de-

223 fined in Fig. 1b using a shapefile drawn in QGIS with a Sentinel-1 image as reference. Polynya area was then calcu-

224 lated by defining any pixel in the study area with a SIC < 70% as being part of the open polynya. The 70% threshold

225 has been commonly used in other studies of polynyas in the summer (e.g. Parmiggiani, 2006; Morelli & Parmig-

226 giani, 2013; Preußer et al., 2015), and the approach has also been used before to calculate winter polynya area

227 (Cheng et al., 2017; 2019). A limitation is that smaller areas of open water that are represented in a pixel dominated

228 by ice-covered area (i.e. > 70%) will not be included in our polynya area value, while ice-covered areas in pixels

229 with SIC < 70% will be included. However, by comparing our SIC data with the SAR imagery we found applying a

230 70% threshold to the SIC data an effective way of capturing winter, as well as summer polynya area in our study

231 area. For example, Fig. 2 b-d shows SAR imagery for a section of the polynya on 21-23 September 2020 and e-g

232 shows the active polynya as identified using a 70% threshold with the SIC data for the same days. To further com-

233 pare the identification of active winter polynya as identified using SIC data with the SAR imagery, we manually

234 identified active polynya in the SAR imagery for the nine days in 2020 when SAR imagery covers the whole ASP

235 study area (green box in Fig. 1b). The results of the comparison can be seen in Fig S1 and generally show good

236 agreement. Note that even if the method was perfect there would be a discrepancy because the measurements are

taken at different times of day and significant changes in active area can occur in hours due to movement of ice, freezing or a mixture of processes. There is also an element of human error in the manual measurement. Of the nine cases, the area was identified as higher using SIC data in five cases and using SAR data in four cases, suggesting that neither approach leads to a systematic over-estimation. Observing Video S2 in comparison to available images in Video S1 also shows the SIC typically effectively captures the presence and variations in area of an active polynya.

While Sentinel-1 imagery has been used to obtain polynya area during the polar night at a higher spatial resolution (40m, Dai et al., 2020), the Bremen SIC product has three key advantages over using Sentinel-1 SAR imagery. First, the SIC product is available daily, in contrast to Sentinel-1 which has many, and sometimes prolonged data gaps over the primary area of interest, particularly during June/July. Given that polynya area can change substantially on a daily or hourly timescale, regular gaps of successive days significantly limits the ability to quantitatively characterize variations throughout the year. Second, several Sentinel-1 images are required to capture the whole ASP study area on a particular day, meaning that even on many days where there are images that are useful for qualitative analysis, the whole polynya cannot be measured. For example, in 2020 there is full coverage of the whole ASP study area for only 22 days with none between 26 April and 12 August, and 9 days in winter (although there are many other days when the whole polynya itself is visible as it does not extend throughout the whole study area). Third, even if sufficient images were available, current methods for calculating polynya area in Sentinel-1 imagery (e.g. Dai et al., 2020) requires manual delimitation which is labor intensive and would be highly time consuming to do for multiple years at a daily temporal resolution. Automated detection of active polynya area in winter using SAR is not yet possible to our knowledge.

3.3 Daily winter ice production

In order to calculate daily ice production in the ASP during the winter periods we followed the approach of Cheng et al. (2017) and utilized their heat flux and ice production model. As input to the model we used atmospheric re-analysis data from the European Centre for Medium-Range Weather Forecasts Reanalysis v5 (ERA5) and the same sea ice concentration data from the University of Bremen described in section 3.2.

Hourly ERA5 data, with a spatial resolution of 31 km, was downloaded from Copernicus (cds.climate.copernicus.eu; Herbach et al., 2018) for the following meteorological variables: air temperature at a height of 2 m, wind speed at a height of 10 m, surface air pressure, dewpoint temperature at a height of 2 m, downward solar radiation and downward thermal radiation. Air temperature, wind speed, surface air pressure and dewpoint temperature were then processed to daily mean values, while solar and thermal radiation were processed to daily cumulative values. These calculations were done for the same ASP study site as for polynya area (Fig. 1b).

3.3.1 Heat Flux Calculation

Following Cheng et al. (2017) the daily net heat flux, Q (in Wm^{-2}), of an active-polynya pixel was estimated by:

274    $Q = (1 − α)R_i + L_i − L_o + F_s + F_e$ (1)

275

276   where R_i (in Wm^{-2}) is the cumulative downward solar radiation; L_i (in Wm^{-2}) is the cumulative downward thermal

277   radiation; L_o (in Wm^{-2}) is the upward thermal radiation; F_s (in Wm^{-2}) and F_e (in Wm^{-2}) are the sensible heat flux

278   and latent heat flux, respectively; and $α$ is the albedo of open water. $α$ was taken to be 0.06 following Cheng et al.

279   (2017; 2019), R_i and L_i were taken from the processed daily ERA5 values and L_o, F_s and F_e were calculated as de-

280   scribed below.

281   The upward thermal radiation was calculated by the Stefan-Boltzmann law:

282

283    $L_o = εσT_s^4$ (2)

284

285   where $ε$ is the longwave emissivity of open water (0.99), and $σ$ is the Stefan–Boltzmann constant (5.67 × 10^{-8}

286   W^{-2}K^{-4}). The temperature of the water surface (T_S, in K), was assumed to be at the freezing point of seawater (T_0 in

287   K), which was calculated following Doherty and Kester (1974) and Cheng et al. (2017; 2019) as:

288

289    $T_S \sim= T_0 = 273.15 − 0.0137 − 0.05199S_w − 0.00007225S_w^2$ (3)

290

291   where S_w (in ‰) is the salinity of sea water. The salinity of the Amundsen Sea was estimated as 34‰ based on Bett

292   et al. (2020).

293   The sensible heat flux, (F_s), and latent heat flux, (F_e) was calculated by:

294

295    $F_s = ρ_ac_pC_sU(T_a − T_0)$ (4)

296

297   and

298

299    $F_e = 0.622ρ_aL_vC_eU(re_a − e_s)/P_0$ (5)

300

301   where $ρ_a$ is the density of air at standard atmospheric pressure and 0°C, taken as, 1.3 kg m^{-3}, c_p is the specific heat of

302   air at constant pressure, taken as 1004 J kg^{-1} K^{-1}, U (in ms^{-1}) is the wind speed at 10 m, taken from the processed

303   ERA5 data and T_a (in K) is the air temperature at 2 m, taken from the processed ERA5 data. C_s and C_e are bulk

304   transfer coefficients for sensible heat and latent heat, respectively and both taken as 0.00144. P_0 (in Pa) is the sur-

305   face air pressure and taken from the processed ERA5 data. L_v (in J kg^{-1}) is the latent heat of water vaporization, r is

306   the relative humidity. E_a (in Pa) is the saturation water vapor pressure at the air temperature, re_a is the actual water

307   vapor pressure of the air and e_s (in Pa) is the saturated water vapor pressure at the surface temperature and are all

308   calculated below:

309

310    $L_v = [2.501 − 0.00237(T_s − 273.15)] × 10^6$ (6),

311

312 $e_s = 611.21 \times 10^{9.8094(T_0-273.15)/(T_0+0.71)}$ (7),

313

314 and

315

316 $re_a = 611.21 \times 10^{9.8094(T_d-273.15)/(T_d+0.71)}$ (8)

317

318 where T_d is the dewpoint temperature taken from the processed ERA5 data.

319

320 **3.3.2 Ice production calculation**

321   The calculated daily heat flux was then cropped, re-aligned, resampled to a 3.125 km^2 grid and reprojected

322 to Antarctic Polar Stereographic using GDAL (Geospatial Data Abstraction Library) and QGIS to match the corre-

323 sponding sea ice concentration data. Next, where SIC was < 0.7 (i.e. pixels considered as part of active polynya)

324 daily ice production volume, V, was estimated in km^3 following Cheng et al. (2017) by the following equation (9).

325 Although ice production will also take place in non-polynya areas where there is ice cover, here we are only con-

326 cerned with ice production taking place in the active polynya.

327

328 $V = 3.125^2(1-SIC)Q/\rho_i L_f$ (9)

329

330 where, as above, SIC is sea ice concentration (as a fraction) and Q is daily net heat flux in W m^{-2}, ρ_i is sea ice den-

331 sity and taken as 920 kg m^{-3} and L_f is the latent heat of sea ice fusion in J kg^{-1}. L_f is calculated following Moham-

332 med and Nirmal (2015) and Cheng et al. (2017) by:

333

334 $L_f = 333400 - 2113(T_0 - 273.15) - 114S_i + 18040S_i/(T_0 - 273.15) + 3.35S_i(T_0 - 273.15) - 3.76(T_0 - 273.15)^2$ (10)

335

336 where S_i is the salinity of sea ice, taken as 6‰ following Cheng et al. (2017).

337   Caution should be used when interpreting the absolute numbers produced by the ice production model, par-

338 ticularly because the input data is reanalysis data not necessarily always representative of reality. This is so because

339 the re-analysis itself is a simulation sensitive to uncertain parameter settings, although it is partly corrected by as-

340 similation of observational data (Cheng et al., 2017; 2019). Also note ERA5 includes a prescribed 'sea ice area frac-

341 tion' parameter that influences the interaction between the atmosphere and ocean in the reanalysis. Nevertheless, we

342 opted for this method due to the difficulty of directly measuring and tracking thin ice thickness in the polynya (e.g.

343 Tian et al., 2020) to estimate ice production, and the potential to compare our daily ice production results to results

344 obtained by the same model for the Ross Ice Shelf Polynya (Cheng et al., 2017; 2019).

345

346 **3.4 Broader spatial changes in SIC**

347   In order to assess changes in the ASP in the context of changes in SIC at a broader spatial scale, SIC was

348   analyzed for the larger area defined in Fig. 1a. The same SIC dataset described in section 2.2 to obtain polynya area

349   was cropped to the broader region. The daily data was plotted spatially for all available days 1 November 2016 – 31

350   March 2021, as shown in Video S2. Monthly mean SIC was also calculated for the whole period and plotted spa-

351   tially. Additionally, the total SIC for each day was calculated by calculating the sum of all percentage SIC values in

352   the study region. These total SIC values should only be considered useful for analyzing relative changes in SIC in

353   our study period.

354

355   **3.5 Wind analysis**

356   In order to analyze the polynya's behavior, we also considered wind conditions. Although a thorough anal-

357   ysis of wind-vector/ice property correlations is beyond the scope of the present paper, which is primarily focused on

358   estimating and describing the variability of the polynya's dynamics, area and ice production, we do consider wind

359   conditions to help inform our analysis of the polynya. Mean daily and annual wind speed and vector winds were cal-

360   culated from hourly ERA5 reanalysis wind products. Hourly zonal (u) and meridional (v) components of vector

361   winds at a height of 10 m were obtained from ERA5 for a region adjacent to the Dotson Ice Shelf and iceberg chain

362   where the polynya typically forms, identified in Fig. S2. Hourly wind speed (V) in ms^{-1} and wind direction (θ) in

363   degrees were calculated as

364

365    $V = (u^2 + v^2)^{1/2}$ (11)

366   and

367    $\theta = tan^{-1} (v/u)$ (12),

368

369   respectively. Daily averaged vector wind fields superimposed on maps of daily averaged wind speed were plotted

370   for the whole study area for the period 1 November 2016 to 31 December 2020 and are included as supplementary

371   video Video S3. A wind rose (Fig. 8) showing the wind speed and direction at times when the active polynya both

372   did not and did increase in area during winter (2017-2020) was also produced for the smaller area (shown by Fig.

373   S2) where the polynya forms from. A map of annual mean vector wind field superimposed on a map of annual mean

374   wind speed was plotted in Fig. 9 .

375   Unfortunately, there is a lack of local observations of wind data in and around the study area with the clos-

376   est station in the United States Antarctic Program's database, on Bear Peninsula, lacking wind data for most of our

377   study period. As a result, some caution should be employed when considering the results obtained from ERA5

378   winds. However, Bracegirdle (2013) and Stammerjohn et al. (2015) note that data from ERA5's predecessor ERA-I

379   in the neighboring Bellingshausen Sea performed better than other reanalysis products.

380

381   **4. Results**

382   In this section, we first summarize our qualitative analysis of the polynya dynamics using Sentinel-1 SAR
383   imagery (Video S1) of the ASP between November 2016 and March 2021 (Section 4.1). Second, we analyze quanti-
384   tative changes in summer (November – March) polynya area for the summers of 2016/17 to 2020/21 (Section 4.2).
385   Third, we analyze quantitative changes in winter (April – October) polynya area and ice production for the winters
386   of 2017 to 2020 (Section 4.3). Fourth, we analyze spatial and temporal wind variations and how they relate to po-
387   lynya area (Section 4.4), and finally, we analyze broader regional patterns in sea ice concentration for the period No-
388   vember 2016 – March 2021 (Section 4.5).
389
390   **4.1 Qualitative analysis of ASP using Sentinel-1 SAR imagery**
391   Typically, in November or early December the polynya transitions from a winter into summer 'mode' as it
392   expands to the west and ice production ceases to take place in the open area i.e. the open polynya area is occupied
393   by open ocean rather than frazil or grease ice (Table 1, Video S1, e.g. Fig 1b). While the polynya's eastern and
394   southern boundaries remain fixed at the Iceberg Chain and coast, respectively, at times during the summer the po-
395   lynya becomes unbound to the west and/or north, and consequently congruent with the open ocean. In the summers
396   of 2018/19 and 2019/20 it remains bound, but in 2016/17 and 2017/18 substantial openings develop in the pack ice
397   boundary. In the summer of 2016/17, particularly from December, the pack ice in the region is notably sparse in
398   comparison to the other years.
399   In February the pack ice around the polynya becomes more extensive and compact, predominantly due to
400   inflow from the Bellingshausen Sea in the north east. As the new pack ice flows into the area it reforms a west-
401   ern/northern boundary to the polynya in the years where a gap had opened, and in all years pushes the existing pack
402   to the east and south-east, reducing the polynya's size. In the exceptionally low-pack ice summer of 2016/17, the
403   newly formed boundary of pack ice is remarkably narrow. In March in all years, new ice production can be seen
404   forming in parts of the polynya and is taking place across all of the polynya by the end of March or early April,
405   marking the polynya's transition into winter 'mode' (Table 1).
406   Throughout the winter, polynya 'events' occur, with existing ice moving away, predominantly to the west
407   off the Iceberg Chain and Thwaites Iceberg Tongue, and new ice forming in the opening (e.g. Figs. 2b-d). On occa-
408   sion the polynya instead forms to the north off the Dotson Ice Shelf. Between April and August, the main polynya
409   appears to primarily have its maximum extent confined to the area adjacent to the Dotson Ice Shelf. Observation of
410   available imagery of polynya events, along with observation of newly-formed polynya ice outflowing from the area,
411   suggests that there is relatively low ice production in these deep winter months. Early and late in the winter, polynya
412   events are sometimes larger, extending further to the west, and there appears to be more associated ice production.
413   After early winter (March/April), as the area becomes more densely covered by inflowing pack ice and
414   newly-formed polynya ice, obstructions occur that appear to limit the evacuation of polynya-produced ice from the
415   vicinity and limit growth of the polynya. Obstructions particularly take place around and adjacent to a group of per-
416   sistently stuck icebergs around the center of the study area that we call the Central Grounded Icebergs around a sea-
417   floor high (Fig. 2a, h). New ice also sometimes becomes stuck (fast) directly adjacent to the south-west of this site
418   (Fig. 2a, h) on another sea-floor high. This intermittently-fast ice blocks outflow from the polynya to the west along

419 the coast, and at times forces new polynya-produced ice to divert around the north of Central Grounded Icebergs

420 (Fig. 2a). An area of grounded icebergs and intermittently-fast ice by Siple Island also sometimes obstructs ice and

421 causes diversions further to the north. All ice produced by the polynya flows to the west overall, eventually rounding

422 the corner of Siple Island.

423   We also observe that, while the overall flow of ice from the ASP is to the west, ice flowing from the po-

424 lynya through the winter 'heaves' and regularly temporarily reverses direction, 'backfilling' eastward into and to-

425 wards the polynya (e.g. Fig 3). This means the polynya sometimes closes through backfilling, and not only through

426 formation and growth of new ice. Back-filling also occur when the polynya does not appear open, meaning that raft-

427 ing and deformation presumably occurs as ice moves back into the polynya zone.

428   A series of smaller polynyas, other than the main polynya that forms off the Iceberg Chain and Dotson Ice

429 Shelf, also form within the study area at times. Mostly notably a 'secondary polynya' forms at times off the Central

430 Grounded Icebergs (Fig. 2a). With inflow of ice from the ASP to this area at times obstructed, as ice moves away

431 from the Central Grounded Icebergs to the west, an opening is created and active ice production is visible. Small

432 polynyas also form at times to the west off the outcrops along the coast.

433
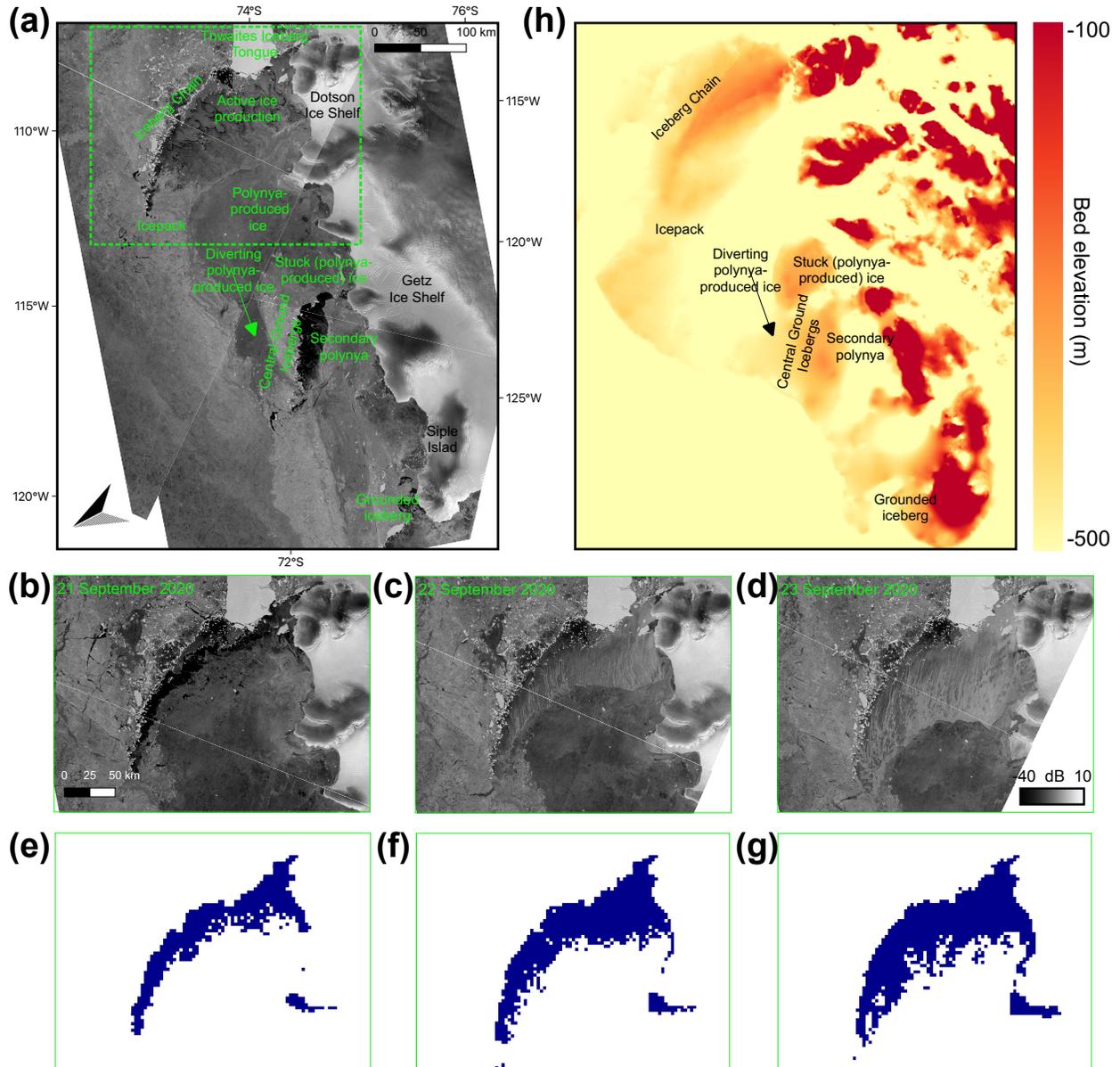
434

435 **Fig. 2. (a)** An example image of the ASP during the winter in a Sentinel-1 SAR image from 5 September 2019. **(b-**

436 **d)** An example of an active polynya event taking place 21-23 September 2020 in Sentinel-1 SAR imagery. Darker

437 ice produced by the ASP can be seen diverting around the Central Grounded Icebergs (and some fast pack ice) after

438 ice became stuck and obstructed outflow along the coast. The area corresponds to the dashed-green box in (a). **(e-g)**

439 Active polynya area (blue) for the same dates and areas as b-d as measured by using a 70% threshold with SIC data

440 **(h)** The elevation of the bed referenced to mean sea level for the same area as (a). The bathymetry data is from the

441 MEaSUREs BedMachine version 2 dataset (Morlighem et al., 2019).

442

443

Year	Polynya opens	Polynya closes
2016/17	8 November 2016*	4 April 2017
2017/18	3 December 2017	9 March 2018
2018/19	13 November 2018	14 March 2019
2019/20	20 November 2019	21 March 2020
2020/21	16 November 2020	8 March 2021

Table 1. Summer polynya opening and closing dates for each summer 2016/17-2020/21 as determined by visual analysis of Sentinel-1 SAR imagery. We determine the polynya to be open for summer when the majority of the open polynya is not exhibiting ice production and closed when the majority of the polynya is exhibiting ice production. * in 2016/17 a lack of imagery in early November means it is difficult to determine when the polynya opened, but it is open by 8 November.
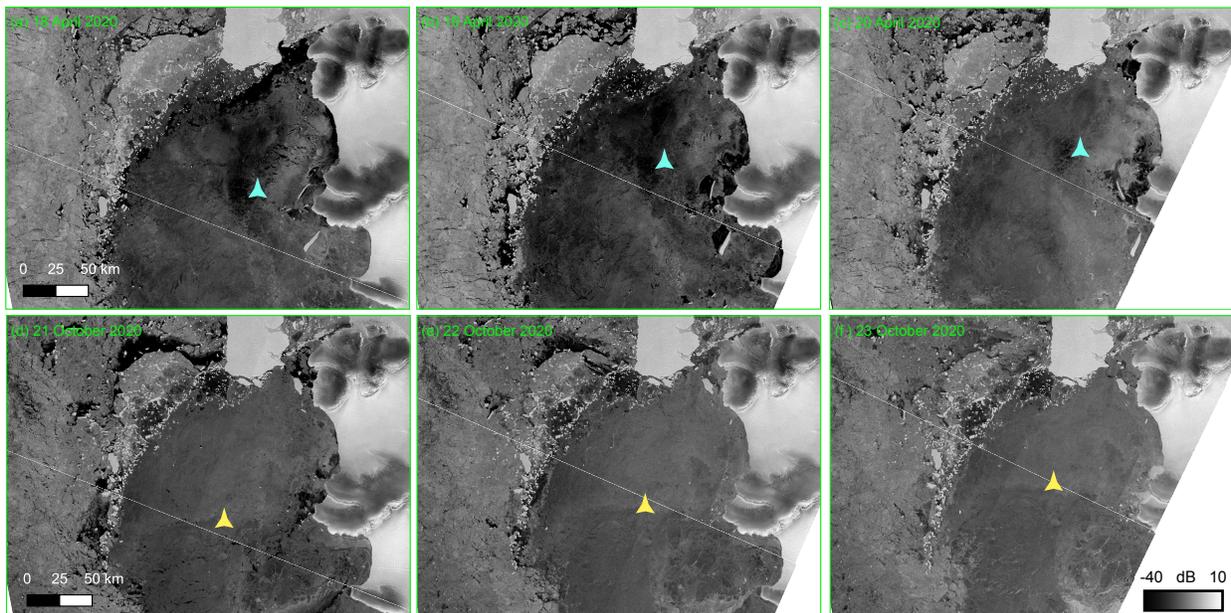
Fig. 3 Examples of 'back-filling', ice earlier produced by the ASP flowing back towards the area adjacent to the Iceberg Chain where it formed. Each box corresponds to the same area shown by the dashed-green box in Fig. 2a, (a-c) show the area on 18-20 April 2020, (d-f) show 21-23 October 2020. The colored shapes in each image are in approximately the same relative position within the ice in each set of images and are to help the reader spot the movement of the ice through the movement of adjacent features. Other examples of back-filling are visible in Video S1.

459
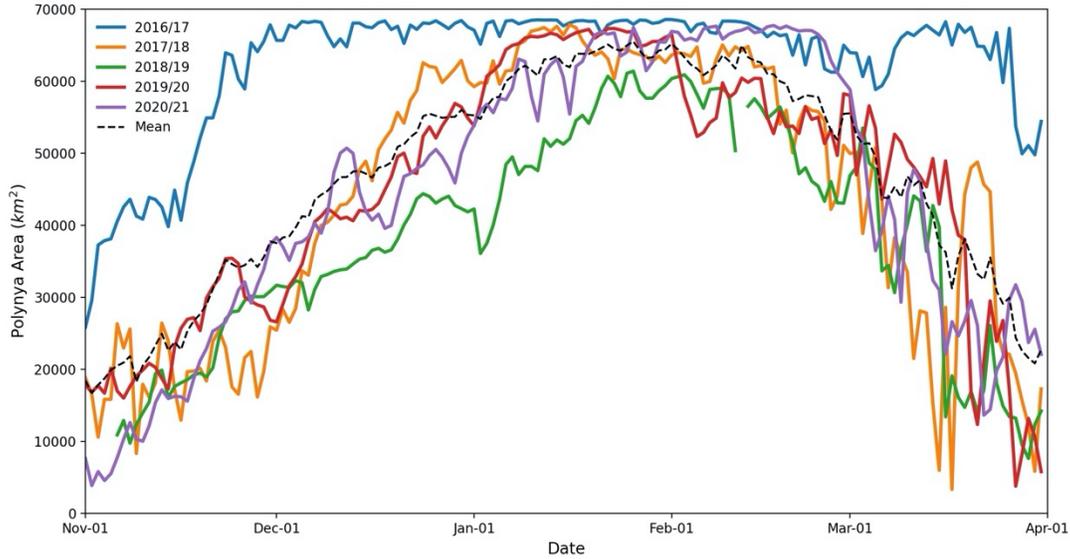
Fig. 4. Daily summer (November-March) polynya area for each summer 2016/17-2020/21 (solid), and the 5-year

461   mean of the daily areas for the whole summer period (dashed).

462

463

4.2 Summer Polynya Area

465   In all years there is an overall increase in polynya area through November (Fig 4). On 1 November, the po-

466   lynya has an area between 7 617 km^2 (2020) and 25 859 km^2 (2016). In the years 2017/18, 2018/19, 2019/20 and

467   2020/21 the polynya area follows a similar pattern, but in 2016/17 it follows a distinct course. By 1 December in

468   2016 the polynya is open in approximately the whole ASP study area, with an area of 65 674 km^2, an increase of

469   154% from 1 November. In 2016/17 the polynya remains open across approximately the whole study area through-

470   out December, January, and most of February and March, only beginning to significantly decline in late March (Fig

471   4) and into April (Fig 5). The polynya in 2016/17 maintains a higher area than in all other years throughout the

472   whole summer, apart from a small period in late February when it is surpassed by 2020/21.

473   In 2017/18, 2018/19, 2019/20 and 2020/21 the polynya area has increased to between 25 439 km^2 (2017)

474   and 38 310 km^2 (2020) by 1 December. From then the polynya continues to follow an overall increasing trend

475   through December, with the polynya reaching its peak area in January in each of these years. In 2018/19 the peak

476   area is substantially lower (61 113 km^2) than in other years, and the polynya only maintains an area above 60 000

477   km^2 for six days in late January and early February. 2018/19 records the lowest area in comparison to other years on

478   every day between 4 December and 3 February. In 2017/18, 2019/20 and 2020/21 the polynya behaves in a similar

479   manner through most the period, with no one of those years consistently recording a higher area, and each year

480   reaching a peak-open area that approximately fills the whole ASP study area. However, polynya area in 2020/21

reaches its peak later (January), and its decline begins later (late February). Notably, in 2017/18 the polynya experiences a temporary rapid re-opening as it increases from just 5 977 km^2 on 15 March to 48 779 km^2 on 21 March. This is an 8.2 fold increase in 6 days, and it is followed by a rapid decline. The polynya had the highest daily mean area for summer (November-March) in 2016/17, at 62 616 km^2, and 2018/19 had the lowest, at 38 518 km^2. The mean daily area of 2017/18, 2019/20 and 2020/21 for summer was 44 013 km^2, 44 979 km^2 and 44 447 km^2, respectively.
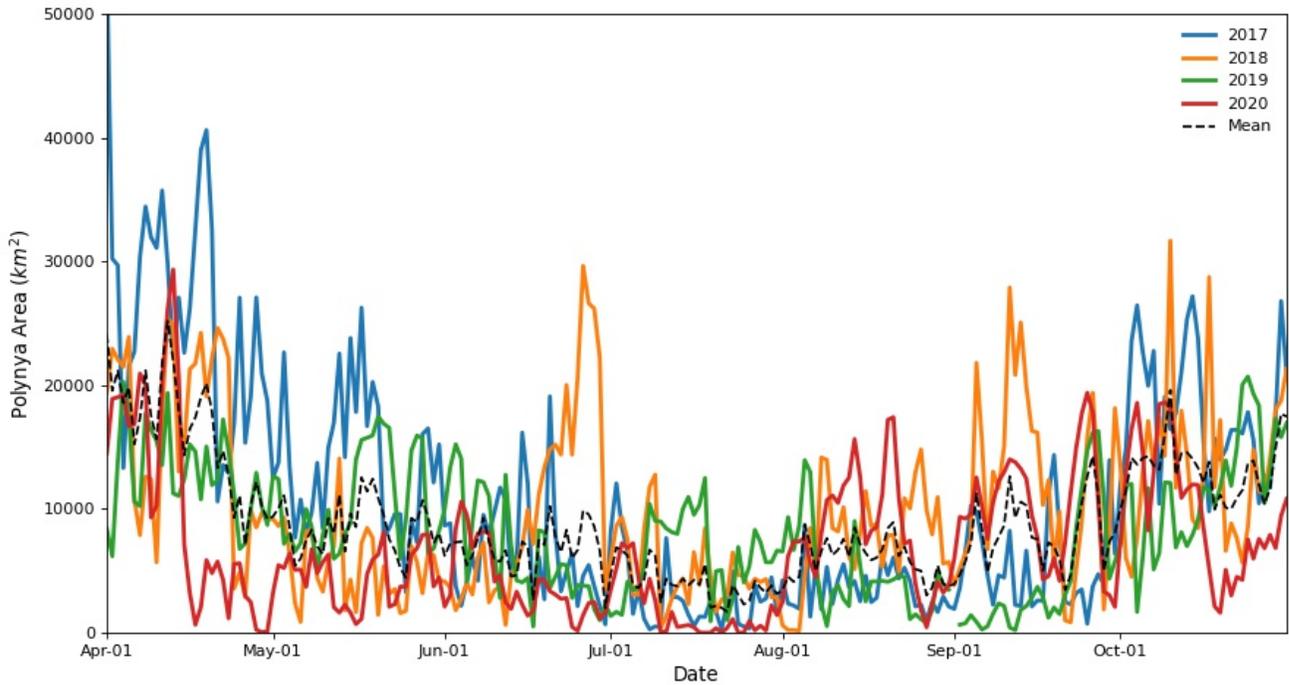
Fig. 5. Daily winter (April-October) polynya area for each winter 2017-2020 (solid), and the 4-year mean of the daily areas for the whole winter period, as measured from AMSR-2 SIC data (dashed).

4.3 Winter Polynya Area and Ice Production

In all years, polynya area exhibits an overall decline from the beginning of the winter period, when the polynya remains relatively large after the summer period (Fig. 5). This period, when the polynya remains relatively large but ice production has now begun, accounts for a substantial proportion of the annual ice production (Fig. 6; Fig. S4). On average, April/May accounts for 36% (39.6 km^3) of annual ice production. The polynya then generally reaches a sustained winter low in area, where it fluctuates around and below 10 000 km^2. In 2020 the polynya area reaches its low in early April, while in 2017, 2019 and mean 2017-20 the area continues an overall decline through April, May and June. Polynya area and ice production then tend to remain low until an increase begins around September. In July polynya area remains below 10 000 km^2 in all years for the whole month apart from brief small fluctuations above this in 2018 and 2019. There are notable spikes in polynya area in the middle of the year, which are also exhibited in spikes in ice production. Most notably in June in 2018 polynya area spikes to 26 631 km^2. After a period of low polynya area, the area generally increases through September and October towards the summer period. In 2020 this period of area and ice production increase begins in August. This late-winter increase in polynya area is

504 also exhibited in a corresponding marked increase in the rate of ice production. On average, September/October ac-
505 counts for 42% (45.8 km^3) of annual ice production.

506   We note that in 2017 between the dates of 1 April and 8 May a substantial portion of the calculated active
507 polynya area, and ice production, occurs in the northwest of the ASP study area. This area is part of the open ocean
508 and is separated by sea ice from the more-typically active polynya area adjacent to the iceberg chain. Typically, ice-
509 pack fills this northwest area, but in early 2017 it is open due to the lack of icepack in this sector in the summer of
510 2016/17, discussed in section 4.3 (Video S2; Fig. 11b).

511   Analysis of the spatial distribution of ice production across all years reveals that the mean daily ice produc-
512 tion is highest in the area of the polynya adjacent to the Iceberg Chain, Thwaites Iceberg Tongue and Dotson Ice
513 Shelf (Fig. 7). Mean annual ice production values (April-October) in this region surpass 17 m^3/m^2. Other notable
514 areas of higher ice production lie along various parts of the coast and an area that corresponds to the secondary po-
515 lynya by the Central Grounded Icebergs.
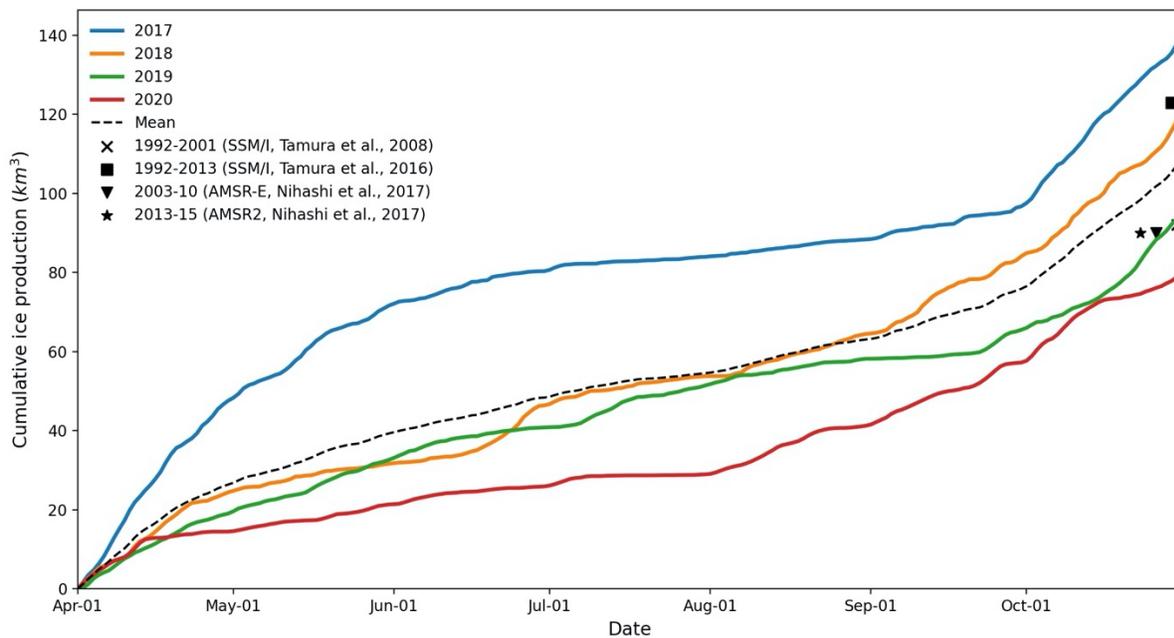
516
517

518 **Fig. 6.** Daily cumulative winter ice production for each winter (April-October) 2017-2020 (solid), and the 4-year
519 mean for the period (dashed), as measured using heat-flux modeling of ERA-5 data and AMSR-2 SIC data. Also
520 shown are mean annual measurements for 1992-2001 (Tamura et al., 2008), 1992-2013 (Tamura et al., 2016), 2003-
521 10 and 2013-15 (Nihashi et al., 2017), along with the instrument used for each measurement. Note the previous stud-
522 ies' measurements covered the period March-October and used a study area that does not exactly correspond to ours.

523

Year	Mean Daily Active Polynya Area (km^2)	Total Annual Ice Production (km^3)	Total Mean Daily Ice Production (km^3)
2017	10 908 (9589)	139	0.67 (0.67)
2018	9 963 (7004)	121	0.57 (0.50)
2019	8 152 (5127)	95	0.45 (0.38)
2020	6 910 (5692)	80	0.38 (0.36)
Mean 2017-20	8 984 (7240)	109	0.52 (0.51)

Table 2. Estimates of Mean Daily Active Polynya Area, Total Annual Ice Production and Mean Daily Ice Production during the winters of 2017-2020, and for the daily mean of the period. Numbers in brackets indicate the standard deviation.
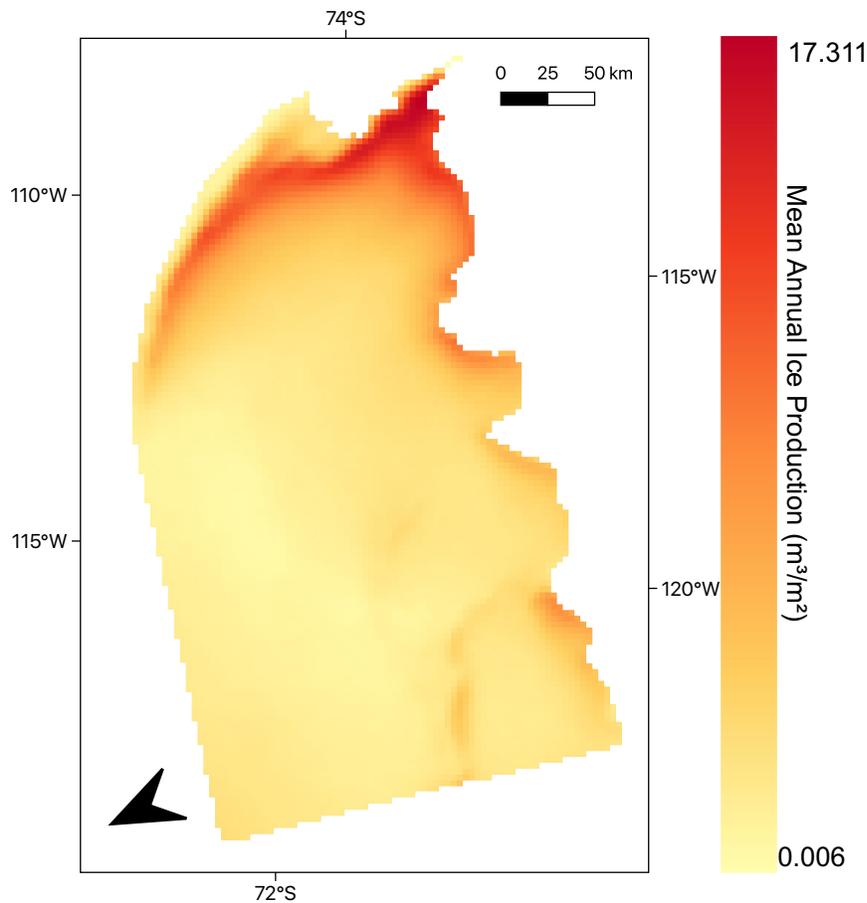
Fig. 7. Mean Annual Ice Production for all winter study periods (April-October 2017-2020). The region corresponds to the region within the green outline in Fig. 1b

4.4 Wind and polynya area

It is clear that polynya events are associated with the presence of strong south-easterly and easterly winds in the region. Figs. 8-9 show that south-easterly and easterly winds dominate the polynya study area. Comparing winter winds in the region where the polynya forms from (Fig. 8; S2) when the active polynya does not increase in area and when it does, shows that while south-easterly winds often occur in both instances, there is a stronger easterly component when an increase in area occurs. The top three wind directions associated with a daily increase in active polynya area are south-easterly, east-south-easterly and easterly, whereas they are south-easterly, southerly and south-south-easterly when area does not increase. Fig. S3 also shows the high density of active polynya area increases with winds with a southerly/easterly winds. It is also visible in Fig. 9 that the location of polynya formation, adjacent to the Dotson Ice Shelf, is associated with a band of high winds with a mean speed of around $8 - 9$ ms^{-1} that extends along the coast from Thwaites Glacier, over the Thwaites Iceberg Tongue and into the south-eastern area of the ASP study area. In the western part of the study area that the polynya extends into, winds tend to be more easterly than south-easterly.
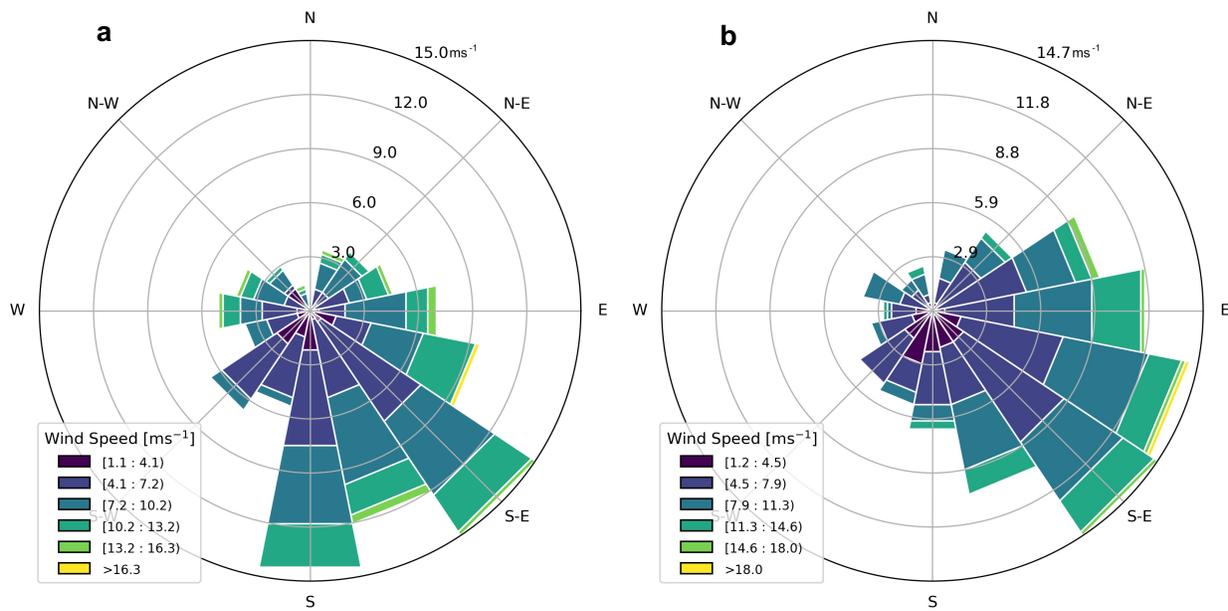
Fig. 8. Wind roses showing the distribution of wind speed and direction during all winters (April-October) in the study period, when the active polynya (a) did not increase in area and (b) did increase in area. These winds are calculated for a region close around that the iceberg chain that the polynya forms from, shown by Fig. S2.

544

545
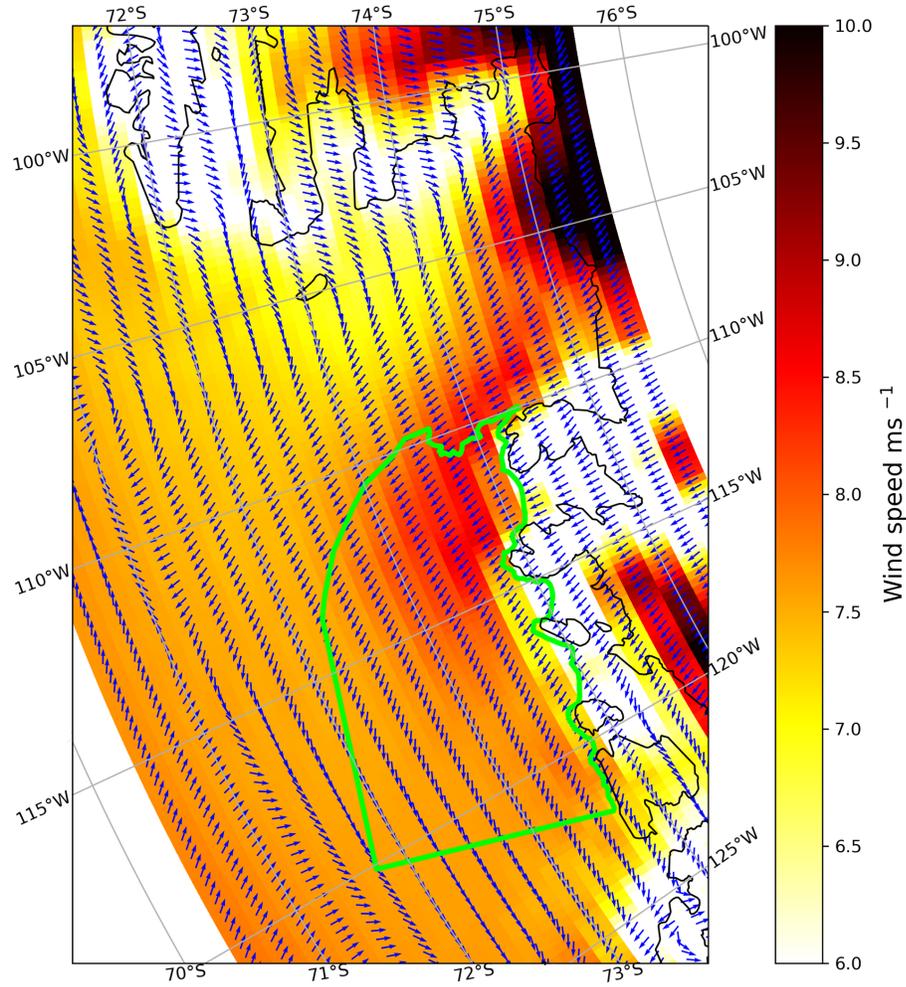
Fig. 9. Annual mean vector wind field and wind speed, calculated for the period 1 November 2016 to 31 December

2020. The green boundary represents the ASP study area, also shown in Fig 1b. Daily maps of vector wind fields

and wind speed are included as Video S3.

549

550

551

552

553
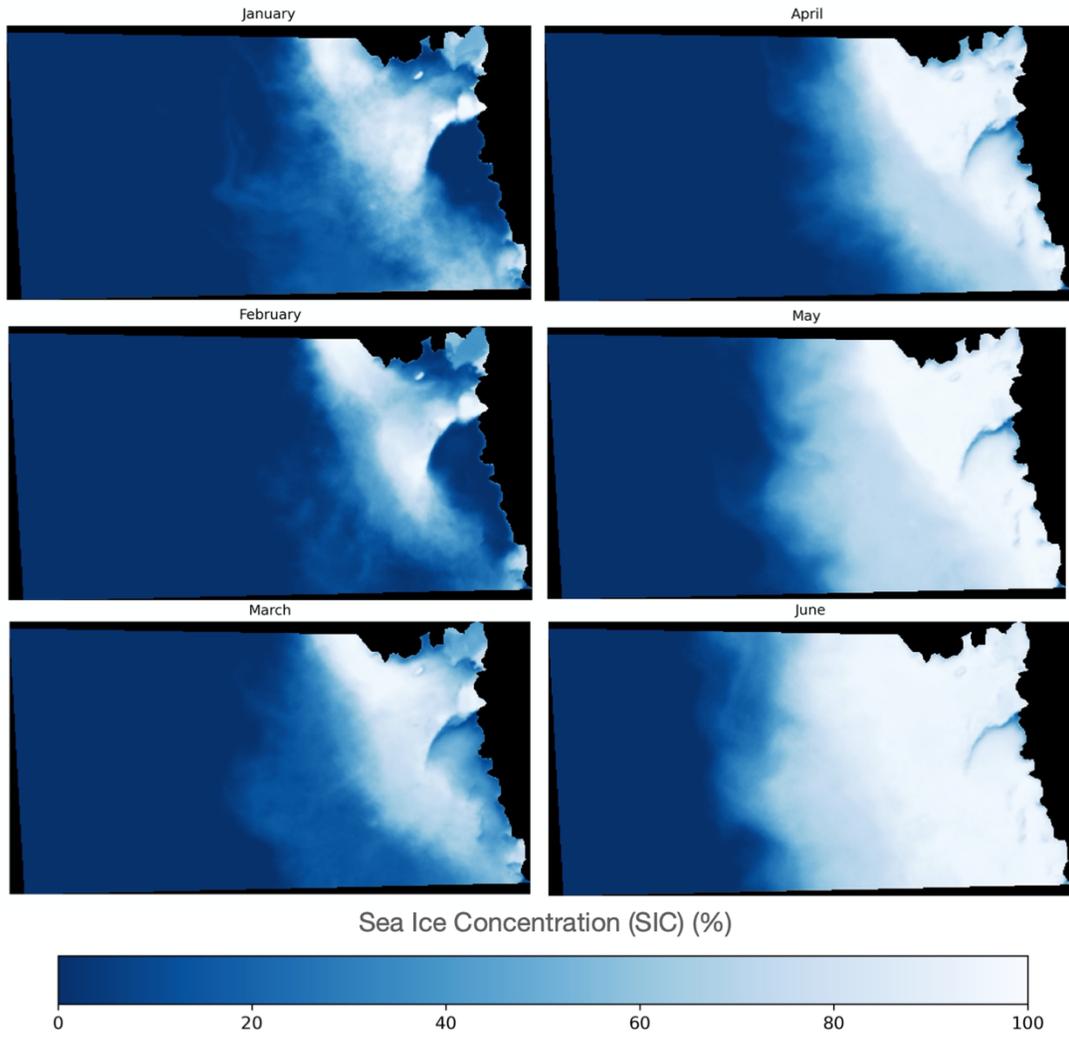
554
555
556
557
558
559
560
561
562
563
564
565
566
567
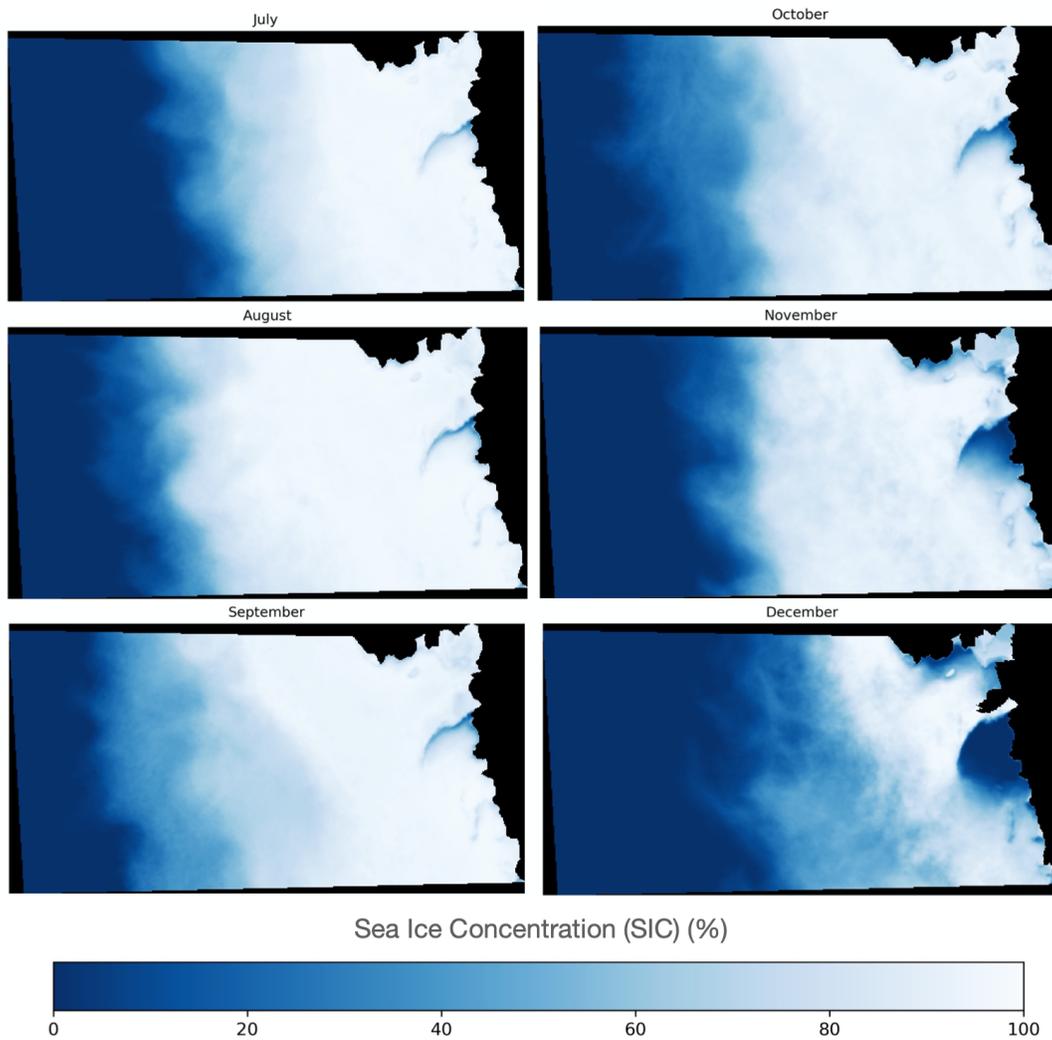
568 **Fig. 10.** Mean monthly SIC for the broader ASP region for the period November 2016 to March 2021. The area cor-
569 responds to that shown by red box in Fig. 1a. Daily data is shown in Video S2.
570
571
572
573
574
575
576
577
578
579
580

581

582
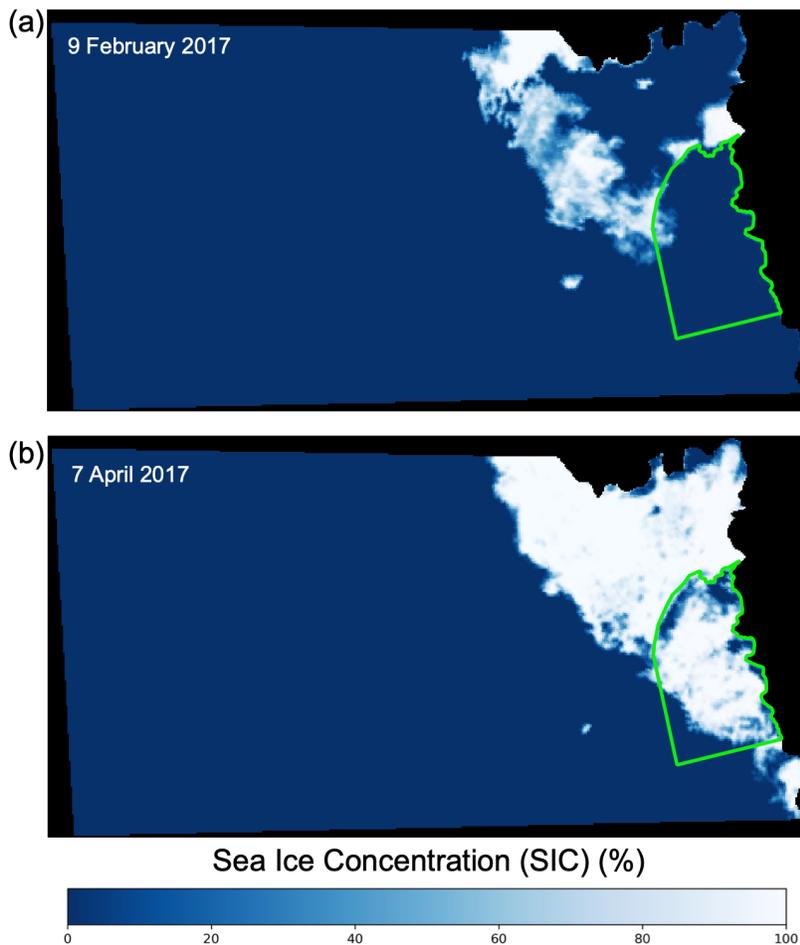
Fig. 11. SIC for the broader ASP region on two days in 2017, during and following a summer of record-low SIC. (a)
An example of when the polynya had no sea ice boundary to the west/north-west due to the exceptionally low SIC in
the region during the 2016/17 summer. (b) An example of the low SIC in the region early in the subsequent winter,
when only a narrow area of pack ice and polynya ice fills the area. The area corresponds to that shown by red box in
Fig. 1a.

588

4.5 Broader SIC

Analysis of the SIC over a broader area also shows daily changes in the polynya area and how it relates to
changes in the icepack. The mean monthly cycle of the polynya can be seen in Fig. 10 and presents a similar picture
of the polynya as described in sections 4.1- 4.3. The broader icepack has a minimum total SIC in January and re-
mains similar in February. From March the broader icepack can be seen to expand in area as the polynya begins to
close and continues to increase until a peak SIC in September. From October the icepack begins a marked decline

595 into summer. Interannual variation can be seen in Fig. S5 and Video S2, with maximum icepack area occurring in
596 August or September each year, and minimum icepack in January or February.

597   During the summer of 2016/17 the icepack is notably sparse (Fig. 11; S5). Around 29 December 2016 a
598 gap in the icepack connects the ASP to the open ocean to north. The icepack continues to diminish and the gap con-
599 necting the ASP to the open ocean broadens until by February the polynya is only bound by part of the Iceberg
600 Chain and Thwaites Iceberg Tongue. The total SIC reaches a minimum on 5 February 2017, 35% of the next lowest
601 annual minimum (2019/20). Gaps in icepack around the Iceberg Chain mean that the ASP has essentially joined
602 with the Pine Island Polynya through the Iceberg Chain for a period in this year. The narrow band of icepack from
603 the east closes the polynya off again in March but the band of adjacent icepack remains so narrow that, as men-
604 tioned, there is open ocean inside our ASP study area until 9 May (Video S2).

605

606   **5. Discussion**

607   Our analysis shows that in some ways the ASP, between November 2016 and March 2021, behaves as is
608 typical for Antarctic coastal polynyas. During the summer the polynya becomes larger and remains ice-free (Fig. 4,
609 Video S1), while during the winter it becomes smaller, opening up during ice-producing polynya 'events' (Figs. 4-5,
610 Video S1). These polynya events and changes in polynya area can sometimes be attributed to higher wind speeds
611 and are often associated with a stronger easterly component in winds close to the iceberg chain (Figs 7-9, S3).

612   Our qualitative analysis of Sentinel-1 SAR imagery, however, also reveals distinct characteristics of the
613 ASP which are not possible to decipher from sea ice concentration data, other quantitative methods, or indirect ob-
614 servation. First, we note that while in many other polynyas, such as the Ross Ice Shelf Polynya, new polynya-pro-
615 duced ice is typically efficiently evacuated away from its origin (Dai et al., 2020), this is not the case at the ASP.
616 Instead, ice formed by the ASP often remains in the ASP study area for months (Video S1). In fact, this polynya-
617 produced ice does not consistently flow in a direction away from the polynya. While its overall direction is west-
618 ward, away from the polynya, the ice 'heaves' and temporarily flows 'backward' ('back-fills') (Fig. 3), as has also
619 been observed at the Mertz Glacier Polynya (Massom et al., 2017). The ice also gets 'stuck' in the region, particu-
620 larly around grounded icebergs, which are grounded in areas where there are topographic highs in the sea floor (Fig.
621 2a, h).

622   The tendency of ice produced by the ASP to remain in the vicinity of the polynya for prolonged periods,
623 become stuck, and sometimes flow back eastward towards the site of its formation, influences the polynya and ice
624 production in two key ways. First, when ice moves eastward while the polynya is active it contributes to the closure
625 of the polynya, and thus the cessation of ice production. Typically, it is assumed that an active polynya during win-
626 ter closes due to new ice production (e.g. Cheng et al., 2017). However, the ASP may close both due to ice produc-
627 tion and movement of previously-produced ice into the polynya. Second, we suggest that the blockages of ice in the
628 vicinity of the polynya reduce the size and frequency of polynya events by hindering the ability of ice to move out of
629 the polynya and open it up. Again, by reducing the size and duration of active polynya area during winter, ice pro-
630 duction is limited.

631   We also note that the ASP forms along the coast westward off a chain of icebergs that extend from the

632   Thwaites Iceberg Tongue. While some polynyas, such as the Ross Ice Shelf polynya, form off and away from the

633   coast, the majority of Antarctic polynyas have been shown to form westward off glacier ice tongues or protruding

634   fast ice (Nihashi et al., 2017). In the case of the ASP, its location and orientation is determined by the presence of

635   the 'Iceberg Chain', which is in turn determined by the presence of a bathymetric high (Figs. 1-2). Stammerjohn et

636   al. (2015) refer to the polynya as forming off a 'fast ice tongue' but we prefer to refer to the 'Iceberg Chain' as the

637   eastern boundary. While a section of fast ice exists amongst, and adjacent to, a section of the southern part of the

638   Iceberg Chain, the extent of this fast ice varies and it only ever extends along a portion of the Iceberg Chain. The

639   Iceberg Chain remains virtually the same length throughout our observations. The polynya consistently forms off the

640   Iceberg Chain regardless of the state or extent of the fast ice. This means that, unlike polynyas that form off variable

641   fast ice (Nihashi et al., 2017), the fundamental morphology of the ASP remains stable through the period. We also

642   note that at no point do we observe significant portions of icepack to 'break through' the Iceberg Chain from the

643   east, regardless of the state of fast ice extent or conditions, and thus the icebergs and the bathymetric high persis-

644   tently 'shield' the polynya from icepack inflow.

645   Another notable feature of the ASP is the development of a 'secondary polynya' during the winter (Fig.

646   2a), where ice production also takes place. This is a polynya that forms within the ASP study area, in an area that is

647   usually part of the main ASP during the summer, but it is not typically congruent with the 'main' polynya during the

648   winter. The polynya forms at the site of the 'Central Grounded Icebergs' and associated 'stuck', transient fast ice.

649   Because some ice has become stuck over the bathymetric high, when adjacent ice drifts away, a polynya activates.

650   This feature again highlights the significance of the bathymetry of the region for sea ice production and dynamics.

651   In line with previous studies of the ASP we find that the ASP is an important site of ice production

652   throughout the winter. Our estimates of annual ice production for 2019 and the mean for 2017-20 fall within the

653   range of predictions by Tamura et al. (2008; 2016) and Ohshima et al. (2017) for 1992-2001/2003-10/2013-15 (90 -

654   117km^3) (Fig. 6). Our estimates for total annual ice production for 2017 (139 km^3) and 2018 (121 km^3) are higher

655   than the highest estimate of those studies, while for 2020 (80 km^3) it is lower. This suggests no significant trend in

656   interannual ice production can be discerned from comparing the period of our study to these previous studies. Some

657   caution must be used in this comparison, however, because those studies include March in ice production calcula-

658   tions and our ASP study area does not exactly correspond to theirs.

659   We find that the shoulder seasons of April/May and September/October are particularly important for ice

660   production due to the higher polynya area at these times, accounting for 36% and 42% of the annual ice production,

661   respectively. This is particularly the case in 2017, when an exceptionally high open polynya area in the summer, due

662   to low icepack conditions (discussed below), continues into the winter period (Figs. 4-6). However, we show that at

663   least some polynya area activates and some ice production occurs throughout the whole winter (Figs. 5-6). Addition-

664   ally, there can be spikes in polynya area and ice production in the deepest winter months. Most notably, polynya

665   area reaches 26 631 km^2 in June. Such isolated, winter events are not reflected in the daily mean for the whole study

666   period, but only when analyzing daily changes for each year (Fig. 5), highlighting the importance of analyzing po-

667   lynya area and ice production at the daily scale to discern important polynya dynamics.

668 When comparing our results to those of Cheng et al. (2017), who used the same method for calculating ice

669 production at the Ross Ice Shelf Polynya, we find that the ASP produces substantially less ice. Between 2003 and

670 2015 they found ice production for the Ross Ice Shelf Polynya was between 164 and 313 km^3 (also for April - Octo-

671 ber) compared to 80 to 139 km^3 for the Amundsen Sea Polynya (this study). This is in line with other studies that

672 compare the two polynyas (Tamura et al. 2008; 2016; Nihashi et al. 2017). We suggest that one limit on polynya

673 area and ice production for the ASP compared to the larger Ross Ice Shelf Polynya, is that the ASP typically forms

674 off the Iceberg Chain. The Iceberg Chain has a stable length of ~190 km, limited by the length of the seafloor sill on

675 which it is grounded, and is an upper limit on the polynya in one dimension. The Ross Ice Shelf Polynya, on the

676 other hand, forms off a coastline, and is only typically limited in this spatial dimension by weather/oceanographic

677 conditions. Another comparative limit on the ASP's ice production is the previously discussed tendency for po-

678 lynya-produced ice to inhibit further activation of the polynya due to blockages and reversals in ice drift. This pro-

679 cess could also partly explain why Cheng et al. (2017) found ice production to remain relatively consistent through-

680 out the winter for the Ross Ice Shelf Polynya, whereas we find ice production for the ASP in June-August to be

681 much lower than in the shoulder months of April/May and September/October.

682 We also note the polynya-produced ice leaves our study area and enters the adjacent sector of the Amund-

683 sen Sea to the west, rather than traveling away from the coast after formation. This westward flow of the ice away

684 from the polynya is likely, in this section, primarily due to the prevalence of easterly winds, especially towards the

685 western part of the study area, and westward ocean currents in the region (Kim et al., 2016; St-Laurent et al., 2019).

686 These ocean currents have been shown to carry icebergs away from our study region, westward through the Amund-

687 sen Sea and into the Ross Sea (Koo et al., 2021). Broader prevailing easterly winds likely play a dominant role in

688 sea ice produced by the ASP eventually drifting to the Ross Sea, as part of a coastal band of westward ice drift (Ass-

689 mann et al., 2005). The fact that the polynya-produced ice remains by the coast may also be influenced by the inflow

690 of older, thicker icepack into our study area. Icepack appears to flow into the region from the Bellingshausen Sea

691 (Video S1, S2) and flows parallel to the ASP-produced ice, potentially playing some role in 'trapping' the ice by the

692 coast. The westward flow of the ice suggests that the level of ice production in the ASP is significant for the adja-

693 cent sector of the Amundsen Sea and the Ross Sea.

694 During the summer we observe the ASP to behave in a similar way in 2016/17 - 2020/21 as Stammerjohn

695 et al. (2015) showed for the period 1979 - 2014. As they did, we find the polynya to open every summer during our

696 study period. We do not note any shift in the location of opening, with the location remaining in the same place as

697 Stammerjohn et al. (2015) noted that it had shifted to in 1992/93. As they did for the years 1992, 1993, 1995, 1997,

698 2003, and 2010, we also note that in 2016/17, there is no icepack adjacent to the ASP in the north and west. This is

699 due to limited advection from the Bellingshausen Sea and Pine Island Polynya, and it causes the ASP to become

700 congruent with the open ocean (Fig. 11). This year was noted as a year of unprecedented springtime retreat and low

701 sea ice concentration for Antarctic sea ice, and was associated with a series of record atmospheric circulation anom-

702 alies and sea surface temperatures (Turner et al., 2017). These broader sea ice conditions caused the polynya to be

703 open in approximately the whole ASP study area through most of the summer in 2016/17, from late November to

704 March. During this time there is also little-to-no distinction between the ASP and the neighboring Pine Island Po-
705 lynya, other than the presence of the Iceberg Chain (Fig. 11a, Video S1). The effect of these extraordinary sea ice
706 conditions in 2016/17 on the polynya in summer, and early winter as mentioned above, may offer insight into how
707 the ASP will behave more commonly in the future if climate change makes such conditions more likely.

708   We note that while Stammerjohn et al. (2015) found the largest polynya area to be February in all but two
709 years during 1979 - 2014, we find the polynya area to be highest in January in each year apart from 2016/17 (when it
710 reaches the peak in November) (Fig. 4). Arrigo et al. (2012) also generally found the polynya area to increase until a
711 later peak in February for the years 1997/98 - 2009/10. While there should be some caution in directly comparing
712 our results with those, due to varying datasets, methods and definitions of the study area, we suggest that a shift in
713 the timing of maximum summer area would promote primary productivity in the polynya. Arrigo et al. (2012) found
714 primary productivity (per unit area) to typically peak in January, and to be declining by the time of the polynya area
715 peak. If the polynya reaches a higher area at an earlier time, when primary productivity is higher, we suggest the
716 potential for primary productivity may be larger during our study period.

717

6. Conclusions

719   Focusing on the summers of 2016/17 - 2020/21 and the winters of 2017 - 2020, we present the first detailed
720 study of year-round variations in the Amundsen Sea Polynya's behavior, area, and ice production. In particular, we
721 take advantage of the recent availability of Sentinel-1 SAR imagery to qualitatively assess the dynamics of the po-
722 lynya through the whole year.

723   Our findings agree with previous studies of earlier periods in finding that the ASP produces a substantial
724 amount of ice through the winter, with some inter-annual variation. We add that the shoulder seasons of April/May
725 and September/October dominate winter ice production, contributing a combined 78%. However, large polynya
726 events, often associated with high winds and a stronger easterly component in wind direction, can occur throughout
727 the winter, promoting significant ice production.

728   The ASP opens each summer in November and closes in March or early April, with peak area typically oc-
729 curring in January. We find that broader regional sea ice conditions can play an important role in the polynya in
730 summer, with the record-low sea ice extent in 2016/17 causing the ASP to become part of the open ocean to the
731 north and join with the Pine Island Polynya to the east.

732   Through our qualitative assessment we identify that the ASP behaves in a distinct manner. The polynya
733 typically forms in a westward direction off a persistent chain of grounded icebergs that are grounded along a bathy-
734 metric high. Ice produced by the polynya is not efficiently evacuated from the site as with other polynyas such as the
735 Ross Ice Shelf Polynya. Instead it stays within the study site, typically for months through the winter, sometimes
736 becoming stuck. This behavior is related to local topographic sea-floor highs which cause icebergs to become
737 grounded and ice to become stuck. At times another smaller 'secondary polynya' forms within the study area adja-
738 cent to grounded icebergs. Relatedly, ice produced by the polynya does not consistently move away from the ASP,
739 instead 'heaving' and sometimes drifting back towards it, contributing to its closure and limiting ice production. Un-
740 like some other polynyas, the polynya-produced ice also drifts westward into other sectors, instead of north, away

from the coast. These behaviors should be accounted for when considering the ASP's influence on the region's sea ice, biology and oceanography.

Given temporal and spatial gaps in Sentinel-1 SAR's coverage, and the difficulty in automating polynya-identification in SAR data, we do not find that it can replace passive microwave or sea ice concentration datasets for analyzing daily changes in polynya area or ice production. However, we find that the ability to directly observe and qualitatively analyze the polynya at a high spatial and temporal resolution, year-round, with Sentinel-1 imagery provides important insights that are not possible with those other datasets. Development of automated approaches to also use Sentinel-1 to quantify high-spatial resolution changes in polynya area and state, such as through machine-learning, could extract more potential from the datasets, particularly for regions with fewer temporal and spatial gaps. Combining such an approach with ice-tracking algorithms to track ice produced by polynya events and measurements of ice thickness (e.g. from satellite altimetry), could help further quantify ice production by polynyas.

Code and Data Availability

Code for data processing and production of figures and videos is available at

https://github.com/geogeordie/AmundsenSeaPolynyaPaper. All processing was done with freely available software, and all data is freely available. Sentinel-1 images were processed in Google Earth Engine or downloaded from: asf.alaska.edu. BedMachine Antarctica V2 was downloaded from: https://nsidc.org/data/nsidc-0756. Sea ice concentration data was downloaded from: http://seaice.uni-bremen.de/. ERA5 climate data was downloaded from: https://cds.climate.copernicus.eu. The MODIS image used for Fig. 1b was downloaded from: https://worldview.earthdata.nasa.gov/

Video Supplement

Video S1: https://doi.org/10.5281/zenodo.5179444

Video S2: https://doi.org/10.5281/zenodo.5179509

Video S3: https://doi.org/10.5281/zenodo.5179590

Author Contributions

GJM primarily conceived the study, processed and analyzed all data and produced all figures, apart from some of the wind processing, analysis, and figures done by AB-C. SFA and AMM-N also contributed to the design of the study and all authors discussed the results and were involved in editing the manuscript.

Competing Interests

The authors declare that they have no conflict of interest.

Financial Support

GJM, SFA and AMM-N were supported by NASA grant #80NSSC19M0194. AB-C was supported by NSERC grant #RGPIN-2022-05217.

778

Acknowledgements

779

We gratefully acknowledge the European Space Agency for making available Sentinel-1 data and the SNAP

780

toolbox, and Google Earth Engine for hosting and processing Sentinel-1 data. We acknowledge the free package

781

Quantarctica, developed by the Norwegian Polar Institute, for use in Fig. 1a. We thank the University of Bremen

782

Sea Ice Remote Sensing Group for processing and making available their sea ice concentration product and the Japa-

783

nese Space Exploration Agency for launching and managing AMSR2. We also acknowledge the ECMWF, NSIDC

784

and NASA for freely-available data. Among others, the free, open-source software packages QGIS, GDAL, Python,

785

NumPy and MatPlotLib were invaluable in this research. We also thank the GIS and StackOverflow StackExchange

786

communities for resources that aided data processing. We thank four anonymous reviewers who reviewed the paper

787

and editor Nicolas Jourdain for suggested revisions.

788

789

References

790

Armstrong, T.: World meteorological organization: WMO sea-ice nomenclature. Terminology, codes and illustrated

791

glossary. J. Glaciol., 11, 148–149. https://doi.org/10.3189/S0022143000022577, 1972.

792

793

Arrigo, K. R., van Dijken, G. L., and Bushinsky, S.: Primary production in the Southern Ocean, 1997–2006, J. Ge-

794

ophys. Res., 113, C08004. https://doi.org/10.1029/2007JC004551, 2008a.

795

796

Arrigo, K. R., van Dijken, G. L., and Long, M.: Coastal Southern Ocean: A strong anthropogenic CO_2 sink. Ge-

797

ophys. Res. Lett., 35, L21602. https://doi.org/10.1029/2008GL035624, 2008b.

798

799

Arrigo, K. R., Lowry, K. E., and van Dijken, G. L.:Annual changes in sea ice and phytoplankton in polynyas of the

800

Amundsen Sea, Antarctica. Deep Sea Research, II 71–76: 5–15. https://doi.org/10.1016/j.dsr2.2012.03.006, 2012.

801

802

Arrigo, K. R. and van Dijken, G. L.: Phytoplankton dynamics within 37 Antarctic coastal polynya systems. J. Ge-

803

ophys. Res., 108, 3271 https://doi.org/10.1029/2002jc001739, 2003.

804

805

Arthur, J. F, Stokes, C. R., Jamieson, S. S. R., Miles, B. W. J., Carr, J. R, and Leeson, A. A.: The triggers of the dis-

806

aggregation of Voyeykov Ice Shelf (2007), Wilkes Land, East Antarctica, and its subsequent evolution. J. Glaciol.

807

https://doi.org/10.1017/jog.2021.45, 2021.

808

809

Assmann, K. M., Hellmer, H. H., and Jacobs, S. S.: Amundsen Sea ice production and transport. J. Geophys. Res.,

810

110, C12013. https://doi.org/10.1029/2004JC002797, 2005.

811

812

Banwell, A. F., Willis, I. C., Macdonald, G. J., Goodsell, B., Mayer, D. P., Powell, A., and MacAyeal, D. R.: Calv-

813

ing and rifting on the McMurdo Ice Shelf, Antarctica. Ann. Glaciol., 58, 78–87. https://doi.org/10.1017/aog.2017.12,

814

2017.

815

816

Bett, D. T., Holland, P. R., Naveira Garabato, A. C., Jenkins, A., Dutrieux, P., Kimura, S., and Fleming, A.: The im-

817

pact of the Amundsen Sea freshwater balance on ocean melting of the West Antarctic Ice Sheet. J. Geophys. Res.:

818

Oceans, 125, e2020JC016305. https://doi.org/10.1029/2020JC016305, 2020.

819

820

Bracegirdle, T. J.: Climatology and recent increase of westerly winds over the Amundsen Sea derived from six rea-

821

nalyses. Int. J. Climatol., 33, 843–851. https://doi.org/10.1002/joc.3473, 2013.

822

823

Bromwich, D. H. and Kurtz, D. D.: Katabatic wind forcing of the Terra Nova Bay polynya. J. Geophys. Res., 89,

824

3561. https://doi.org/10.1029/JC089iC03p03561, 1984.

825

826

827   Bromwich, D., Liu, Z., Rogers, A. N., and Van Woert, M. L.: Winter atmospheric forcing of the Ross Sea polynya.
828   Ocean ICE Atmos. Int. Antarct. Cont. Margin, 75, 101-133. https://doi.org/10.1029/AR075p0101, 1998.
829

830   Bromwich, D. H., Carrasco, J. F., Liu, Z., and Tzeng, R. Y.: Hemispheric atmospheric variations and oceanographic
831   impacts associated with katabatic surges across the ross ice shelf, Antarctica. J. Geophys. Res.-Atmos, 98, 13045-
832   13062. https://doi.org/10.1029/93JD00562, 1993.
833

834   Budge, J. S. and Long, D. G.: A comprehensive database for Antarctic iceberg tracking using scatterometer data.
835   IEEE JSTARS 11(2), 434-442. https://10.0.4.85/JSTARS.2017.2784186, 2018.
836

837   Cheng, Z., Pang, X., Zhao, X., and Tan, C.: Spatio-Temporal Variability and Model Parameter Sensitivity Analysis
838   of Ice Production in Ross Ice Shelf Polynya from 2003 to 2015. Remote Sensing, 9, 934.
839   https://doi.org/10.3390/rs9090934, 2017.
840

841   Cheng, Z., Pang, X., Zhao, X., and Stein, A.: Heat Flux Sources Analysis to the Ross Ice Shelf Polynya Ice Produc-
842   tion Time Series and the Impact of Wind Forcing, Remote Sensing, 11, 188. https://doi.org/10.3390/rs11020188,
843   2019.
844

845   Dai, L., Xie, H., Ackley, S. F., and Mestas-Nuñez, A. M.: Ice Production in Ross Ice Shelf Polynyas during 2017–
846   2018 from Sentinel–1 SAR Images. Remote Sensing, 12, 1484. https://doi.org/10.3390/rs12091484, 2020.
847

848   Doherty, B. T. and Kester, D. R.: Freezing Point of Seawater. J. Mar. Res., 32, 285-300. 1974.
849

850   Drucker, R., Martin, S., and Kwok, R..: Sea ice production and export from coastal polynyas in the Weddell and
851   Ross Seas. Geophys. Res. Lett., 38, L1705. https://doi.org/10.1029/2011GL048668, 2011.
852

853   Environment Canada.: Manual of Standard Procedures for Observing and Reporting Ice Conditions (MANICE), Me-
854   teorological Service of Canada, 2005. [Available at: https://publications.gc.ca/collections/collection_2013/ec/En56-
855   175-2005-eng.pdf]
856

857   Greene, C. E., Young, D. A., Gwyther, D. E., Galton-Fenzi, B. E., and Blankenship, D. D.: Seasonal dynamics of
858   Totten Ice Shelf controlled by sea ice buttressing. Cryosphere, 12, 2869-2882. https://doi.org/10.5194/tc-12-2869-
859   2018, 2018.
860

861   Grossmann, S. and Dieckmann, G. S.: Bacterial Standing Stock, Activity, and Carbon Production during Formation
862   and Growth of Sea–Ice in the Weddell Sea, Antarctica. Appl. Environ. Microb., 60, 2746–2753.
863   https://doi.org/10.1128/aem.60.8.2746-2753.1994, 1994.
864

865   Hersbach, H., Bell, B., Berrisford, P., Biavati, G., Horányi, A., Muñoz Sabater, J., Nicolas, J., Peubey, C., Radu, R.,
866   Rozum, I., Schepers, D., Simmons, A., Soci, C., Dee, D., and Thépaut, J.-N.: ERA5 monthly averaged data on single
867   levels from 1979 to present. Copernicus Climate Change Service (C3S) Climate Data Store (CDS). (Accessed on <
868   01-04-2021), https://doi.org/10.24381/cds.f17050d7, 2019.
869

870   Hollands, T. and Dierking, W.: Dynamics of the Terra Nova Bay Polynya: The potential of multi-sensor satellite
871   observations, Remote Sens. Environ., 187, 30–48, https://doi.org/10.1016/j.rse.2016.10.003, 2016
872

873   IMBIE team: Mass balance of the Antarctic ice sheet from 1992 to 2017. Nature 558, 219-222.
874   https://doi.org/10.1038/s41586-018-0179-y, 2018.
875

876   Ito, M., Ohshima, K. I., Fukamachi, Y., Mizuta, G., Kusumoto, Y., and Nishioka, J.: Observations of frazil ice for-
877   mation and upward sediment transport in the Sea of Okhotsk: A possible mechanism of iron supply to sea ice. J. Ge-
878   ophys. Res.–Oceans, 122, 788–802. https://doi.org/10.1002/2016JC012198, 2017.
879

880   Kim, C.-S., Kim, K.-W., Cho, K.-H., Ha, H. K., Lee, S.H., Kim, H.-C., Lee, J.-H.: Variability of the Antarctic
881   Coastal Current in the Amundsen Sea. Estuar. Coast. Shelf S., 181, 123–133,
882   https://doi.org/10.1016/j.ecss.2016.08.004, 2016.

883
884 Kimura, N. and Wakatsuchi, M.: Increase and decrease of sea ice area in the Sea of Okhotsk: Ice production in
885 coastal polynyas and dynamic thickening in convergence zones. J. Geophys. Res.-Oceans, 109, C09S03.
886 https://doi.org/10.1029/2003JC001901, 2004.
887
888 Koo, Y., Xie, H., Ackley, S. F., Mestas-Nuñez, A. M., Macdonald, G. J., and Hyun, C.-U.: Semi-automated tracking
889 of iceberg B43 using Sentinel-1 SAR images via Google Earth Engine. Cryosphere., 15, 4727–4744,
890 https://doi.org/10.5194/tc-15-4727-2021, 2021.
891
892 Lee, S.H., Hwang, J., Ducklow, H. W., Hahm, D., Lee, S. H., Kim, D., Hyun, J.-H., Park, J., Ha, H. K., Kim, T. W.,
893 Yang, E. J., Shin, H. C.: Evidence of minimal carbon sequestration in the productive Amundsen Sea polynya, Ge-
894 ophys. Res. Lett., 44, 15, 7892-7899. https://doi.org/10.1002/2017GL074646, 2017.
895
896 Massom, R. A., Hill, K. L., Lytle, V. I., Worby, A.P., Paget, M. J., and Allison, I.: Effects of regional fast-ice and
897 iceberg distributions on the behaviour of the Mertz Glacier polynya, East Antarctica. Ann. Glaciol., 33, 391-398.
898 https://doi.org/10.3189/172756401781818518, 2001.
899
900 Massom, R. A., Scambos, T. A., Bennetts, L. G., Reid, P., Squire, V. A., and Stammerjohn, S. E.: Antarctic ice shelf
901 disintegration triggered by sea ice loss and ocean swell. Nature, 558, 383-389. https://doi.org/10.1038/s41586-018-
902 0212-1, 2018.
903
904 Matsuoka, K., Skoglund, A., Roth, G., de Pomereu, J., Griffiths, H., Headland, R., Herried, B., Katsumata, K., Le
905 Brocq, A., Licht, K., Morgan, F., Neff, P. D., Ritz, C., Scheinert, M., Tamura, T., Van de Putte, A., van den Broeke,
906 M., von Deschwanden, A., Deschamps-Berger, C., Van Liefferinge, B., Tronstad, S., and Melvær, Y.: Quantarctica,
907 an integrated mapping environment for Antarctica, the Southern Ocean, and sub-Antarctic islands. Environ. Modell.
908 Softw., 140, 105015. https://doi.org/10.1016/j.envsoft.2021.105015, 2021.
909
910 Mazur, A. K., Wåhlin, A. K., Kręzel, A.: An object-based SAR image iceberg detection algorithm applied to the
911 Amundsen Sea, Remote Sens. Environ., 189, 67–83, https://doi.org/10.1016/j.rse.2016.11.013, 2017.
912
913 Mazur, A. K., Wåhlin, A. K., and Kalén, O.: The life cycle of small-to medium-sized icebergs in the Amundsen sea
914 embayment, Polar Res., 38, 1–17, https://doi.org/10.33265/polar.v38.3313, 2019.
915
916 Moore, G. W. K., Howell, S. E. L., and Brady, M.: First observations of a transient polynya in the Last Ice Area
917 north of Ellesmere Island. Geophys. Res. Lett., 48, e2021GL095099. https://doi.org/10.1029/2021GL095099, 2021.
918
919 Morales Maqueda, M. A., Willmott, A. J., and Biggs, N. R. T.: Polynya dynamics: a review of observations and
920 modeling, Rev. Geophys., 42, RG1004. https://doi.org/10.1029/2002RG000116, 2004.
921
922 Morelli, S. and Parmiggiani, F.: Wind over Terra Nova Bay (Antarctica) during a polynya event: Eta model simula-
923 tions and satellite microwave observations. Eur. Phys. J. Plus 128, 135 (2013). https://doi.org/10.1140/epjp/i2013-
924 13135-8, 2013.
925
926 Morlighem, M.: MEaSUREs BedMachine Antarctica, Version 2. Boulder, Colorado USA. NASA National Snow
927 and Ice Data Center Distributed Active Archive Center. https://doi.org/10.5067/C2GFER6PTOS4, 2019. [Date Ac-
928 cessed: 01-04-2021].
929
930 Nakata, K., Ohshima, K. I., and Nihashi, S.: Estimation of thin ice thickness and discrimination of ice type from
931 AMSR-E passive microwave data. IEEE TGRS, 57(1), 263–276. https://doi.org/10.1109/TGRS.2018.2853590,
932 2019.
933
934 Nakata, K., Ohshima, K. I., and Nihashi, S.: Mapping of active frazil for Antarctic coastal polynyas, with an estima-
935 tion of sea-ice production. Geophys. Res. Lett., 48, e2020GL091353. https://doi.org/10.1029/2020GL091353, 2021.
936

937 Nihashi, S., and Ohshima, K. I.: Circumpolar Mapping of Antarctic Coastal Polynyas and Landfast Sea Ice: Rela-
938 tionship and Variability, J. Climate, 28, 3650-3670. https://doi.org/10.1175/JCLI-D-14-00369.1, 2015.
939
940 Nihashi, S., Ohshima, K. I., and Tamura, T.: Sea-Ice Production in Antarctic Coastal Polynyas Estimated From
941 AMSR2 Data and Its Validation Using AMSR–E and SSM/I–SSMIS Data. IEEE JSTARS, 10, 3912-3922.
942 https://doi.org/10.1109/JSTARS.2017.2731995, 2017.
943
944 Ohshima, K. I., Fukamachi, Y., Williams, G. D., Nihashi, S., Roquet, F., Kitade, Y., Tamura, T., Hirano, D., Her-
945 raiz-Borreguero, L., Field, I., Hindell, M., Aoki, S. and Wakatsuchi, M. L.: Antarctic Bottom Water production by
946 intense sea–ice formation in the Cape Darnley polynya. Nat. Geosci., 6, 235-240. https://doi.org/10.1038/ngeo1738,
947 2013.
948
949 Park, J., Kim, H.-C., Jo, Y.-H., Kidwell, A., and Hwang, J.: Multi-temporal variation of the ross sea polynya in re-
950 sponse to climate forcings. Polar Res., 37, 1444891. https://doi.org/10.1080/17518369.2018.1444891, 2018.
951
952 Parkinson, C. L.: A 40-y record reveals gradual Antarctic sea ice increases followed by decreases at rates far exceed-
953 ing the rates seen in the Arctic. P. Natl. Acad. Sci. U.S.A., 116, 14414-14423.
954 https://doi.org/10.1073/pnas.1906556116, 2019.
955
956 Parmiggiani, F.: Fluctuations of Terra Nova Bay polynya as observed by active (ASAR) and passive (AMSR-E) mi-
957 crowave radiometers, Int. J. Remote. Sens., 27:12, 2459 2467. https://doi.org/10.1080/01431160600554355, 2007.
958
959 Preußer, A., Heinemann, G., Willmes, S., and Paul, S.: Multi-Decadal Variability of Polynya Characteristics and Ice
960 Production in the North Water Polynya by Means of Passive Microwave and Thermal Infrared Satellite Imagery.
961 Remote Sensing, 7, 15844-15867. https://doi.org/10.3390/rs71215807, 2015.
962
963 QGIS.org: QGIS Geographic Information System. QGIS Association. http://www.qgis.org. 2021.
964
965 Rack, W., Price, D., Haas, C., Langhorne, P. J., and Leonard, G. H.: Sea Ice Thickness in the Western Ross Sea. Ge-
966 ophys. Res. Lett., 48, e2020GL090866. https://doi.org/10.1029/2020GL090866, 2020.
967
968 Rignot, E., Mouginot, J., Scheuchl, B., van den Broeke, M., van Wessem, M. J., and Morlighem, M.: Four decades
969 of Antarctic ice sheet mass balance from 1979–2017. P. Natl. Acad. Sci. U.S.A. 116, 1095-1103.
970 https://doi.org/10.1073/pnas.1812883116, 2019.
971
972 Sansiviero, M., Morales Maqueda, M. Á., Fusco, G., Aulicino, G., Flocco, D., and Budillon, G.: Modelling sea ice
973 formation in the Terra Nova Bay polynya. J. Marine Syst., 166, 4-25. https://doi.org/10.1016/j.jmarsys.2016.06.013,
974 2017.
975
976 Spreen, G. Kaleschke, G. L, and Heygster, G.: Sea ice remote sensing using AMSR-E 89 GHz channels. J. Geophys.
977 Res., 113, C02S03. https://doi.org/10.1029/2005JC003384, 2008.
978
979 Stammerjohn, S. E., Maksym, T., Massom, R. A., Lowry, K. E., Arrigo, K. R., Yuan, X., Raphael, M., Randall-
980 Goodwin, E. R., Sherrell, R. M., and Yager, P. L.: Seasonal sea ice changes in the Amundsen Sea, Antarctica, over
981 the period of 1979–2014. Elementa: Science of the Anthropocene, 3, 000055. https://doi.org/10.12952/journal.ele-
982 menta.000055, 2015.
983
984 St-Laurent, P., Yager, P. L., Sherrell, R. M., Stammerjohn, S. E., and Dinniman, M. S.: Pathways and supply of dis-
985 solved iron in the Amundsen Sea (Antarctica), J. Geophys. Res.-Oceans, 122, 7135–7162, https://doi.org/10.1002/
986 2017JC013162, 2017.
987
988 St-Laurent, P., Yager, P. L., Sherrell, R. M., Oliver, H., Dinniman, M. S., and Stammerjohn, S. E.: Modeling the
989 seasonal cycle of iron and carbon fluxes in the Amundsen Sea Polynya, Antarctica. J. Geophys. Res.: Oceans, 124,
990 1544–1565. https://doi.org/10.1029/2018JC014773, 2019.
991

992 Sweeney, C.: The annual cycle of surface water CO2 and O2 in the Ross Sea: A model for gas exchange on the con-
993 tinental shelves of Antarctica, in Biogeochemistry of the Ross Sea. Antarctica Research Series, 78, edited by Dun-
994 bar, R. B., and DiTullio, G. R., pp. 295-312, AGU, Washington, D. C., 2003.
995
996 Tamura, T., Ohshima, K. I., and Nihashi, S.: Mapping of sea ice production for Antarctic coastal polynyas, Ge-
997 ophys. Res. Lett., 35, L07606. https://doi.org/10.1029/2007GL03290, 2008.
998
999 Tamura, T., Williams, G. D., Fraser, A. D., and Ohshima, K. I.: Potential regime shift in decreased sea ice produc-
1000 tion after the Mertz Glacier calving. Nat. Commun., 3, 826. https://doi.org/10.1038/ncomms1820, 2012.
1001
1002 Tian, L., Xie, H., Ackley, S. F., Tang, J., Mestas-Nuñez, A. M., and Wang, X.: Sea-ice freeboard and thickness in
1003 the Ross Sea from airborne (IceBridge 2013) and satellite (ICESat 2003-2008) observations. Ann. Glaciol., 61(82),
1004 24-39. https://doi.org/10.1017/aog.2019.49, 2020.
1005
1006 Webber, B. G. M., Heywood, K. J., Stevens, D. P., Dutrieux, P., Povl Abrahamsen, E., Jenkins, A., Jacobs, S. S.,
1007 Ha, H. K., Lee, S. H., and Kim, T. W.: Mechanisms driving variability in the ocean forcing of Pine Island Glacier,
1008 Nat. Commun., 8, 14507. https://doi.org/10.1038/ncomms14507, 2017.